Spin liquids and frustrated magnetism

J. T. Chalker
Theoretical Physics. Oxford University, 1, Keble Road, Oxford, OX1 3NP

Lecture notes for lectures at École de Physique des Houches, August 2104.

1 Introduction

Two important markers in the history of research on spin liquids and frustrated magnetism are Anderson's suggestion [1], over 40 years ago, of the resonating valence bond state as an alternative to Néel order, and Ramirez' influential review[2], some 20 years ago, of strongly frustrated magnets. There has been a tremendous amount of progress since then but much remains to be done, especially in identifying experimental examples of spin liquids and understanding their properties. In these lecture notes I aim to provide an introduction to the field that links our understanding of the classical statistical physics of these systems with approaches to their quantum mechanics. Short complementary introductions can be found in the articles by Lee [3] and by Balents [4]; more specialised reviews of various aspects of the field can be found in a recent book[5]; and alternative approaches to the one taken in the present notes are outlined in Section 6.

The term *spin liquid* is presumably intended to draw an analogy between possible states of a magnet and the conventional three phases of matter, but this analogy fails to capture some of the most interesting features of spin liquids. More specifically, it is reasonable to see a paramagnet as being like a gas, since both states occur at high temperature and are essentially uncorrelated; and it is also appropriate to think of a Néel state as like a solid, in the sense that both have broken symmetry, characterised by a local order parameter, and occur at low temperature. But whereas classical fluids have only local correlations, we shall see that classical spin liquids may have a divergent correlation length and power-law correlations. And in place of the Fermi surface or Bose condensate of quantum fluids, quantum spin liquids may have topological order and fractionalised excitations.

1.1 Overview

We will be concerned with the statistical mechanics and quantum mechanics of models for magnetic degrees of freedom in Mott insulators. These have well-defined local moments which we represent using simple spin Hamiltonians such as the Ising and Heisenberg models. The models are said to be frustrated if different contributions to the interaction energy have conflicting classical minima. The interest of frustration in these systems is that it acts to destabilise conventional ordered states. Classically, one sees this from a large contribution to ground-state degeneracy, which is *accidental* in the technical sense that it is not a consequence of symmetry.

The ideas of frustration and accidental degeneracy can be illustrated by considering a cluster of spins with antiferromagnetic interactions between all pairs in the cluster. To allow some generality, we take a cluster of q classical spins, represented using n-component unit vectors $\mathbf{S}_i$. The Hamiltonian

$$\mathcal{H} = J\sum_{\langle ij\rangle} \mathbf{S}_i \cdot \mathbf{S}_j = \frac{J}{2}|\mathbf{L}|^2 + \text{const.} \quad \text{with} \quad \mathbf{L} = \sum_{i=1}^{q} \mathbf{S}_i \tag{1}$$

(where $\sum_{\langle ij\rangle}$ denotes a sum over pairs ij) is minimised in states for which the total magnetisation $\mathbf{L}$ of the cluster is zero. When $q > 2$, no state can minimise the interaction energy $J\,\mathbf{S}_i \cdot \mathbf{S}_j$ of all pairs simultaneously. For example, a set of four Ising spins with nearest neighbour antiferromagnetic interactions on a tetrahedron hence has a ground state in which two spins are up and two are down. This gives a ground-state degeneracy of six, rather than the generic value of two for Ising systems with time-reversal symmetry. Replacing these Ising spins with classical Heisenberg spins, the ground states (as illustrated in Fig. 1) have two internal degrees of freedom in addition to the three that arise from global rotations of any non-collinear spin arrangement.

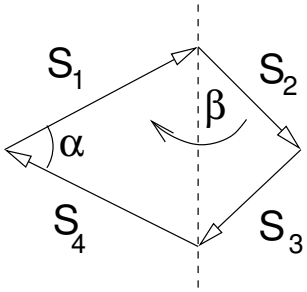

Figure 1: Ground states of four antiferromagnetically coupled classical Heisenberg spins: the two accidental ground-state degrees of freedom are the angle α between spins $\mathbf{S}_1$ and $\mathbf{S}_4$, and the angle β between the plane containing $\mathbf{S}_1$ and $\mathbf{S}_4$, and that containing $\mathbf{S}_2$ and $\mathbf{S}_3$.

Some of the most important lattices for the study of geometrically frustrated magnets can be constructed as corner-sharing arrangements of clusters: examples are the kagome and pryrochlore lattices, formed in this way from triangles or tetrahedra and shown in Fig. 2.

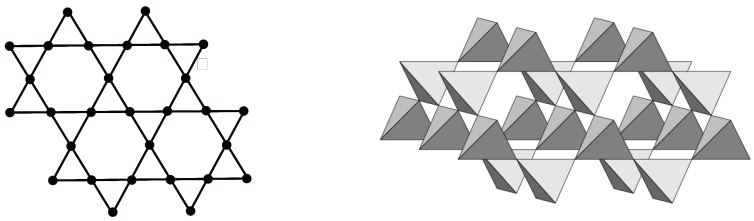

Figure 2: Two lattices: the kagome (left) and the pyrochlore (right).

It is useful for orientation to discuss the some selected examples of geometrically frustrated magnetic materials, listed in Table 1, although we will not attempt any sort of survey. An important characterisation is provided by the dependence of the magnetic susceptibility $\chi(T)$ on temperature T. At high temperatures it obeys the Curie-Weiss law

$$\chi(T) \propto \frac{1}{T - \theta_{\rm CW}} \tag{2}$$

and the magnitude of the Curie-Weiss constant $\theta_{\rm CW}$ (negative if exchange is antiferromagnetic) reflects the energy scale of exchange interactions. Without frustration, one expects ordering at a temperature scale set by $|\theta_{\rm CW}|$. By contrast, highly frustrated systems remain in the paramagnetic phase to much lower temperatures, and in some cases to zero temperature. Their low-temperature fate may involve freezing or a structural, frustration-relieving transition at temperature $T_{\rm c}$, and Ramirez introduced the ratio

$$f = -\frac{\theta_{\rm CW}}{T_{\rm c}} \tag{3}$$

as a simple measure for the degree of frustration. The state of a system in the temperature range $|\theta_{\rm CW}| \gg T > T_{\rm c}$, where spins are highly correlated but strongly fluctuating, was termed by Villain [6] a *cooperative paramagnet*. This is the spin liquid state we wish to characterise more thoroughly, at both the classical and the quantum levels.

These ideas are illustrated by the first material in our selection, SCGO. It has a frustration parameter $f \gtrsim 100$ [7] and magnetic neutron scattering shows strong spin correlations at low temperature (via a peak in scattering at intermediate wavevector) but no long-range order (from the absence of magnetic Bragg peaks) [8]. To obtain more detailed information about low-temperature spin correlations using neutron scattering requires single crystals. These are not available for SCGO, but for spin-ice materials so-called *pinch-point* features in the diffuse scattering [9], which are sharp in reciprocal space, reveal long-range correlations in real space (see Section 4 and lectures at this summer school by B. Gaulin).

The other listed materials, herbertsmithite and κ-ET, are two of the best candidate quantum spin liquids. Neither shows signs of magnetic order, even at the lowest accessible temperatures. Moreover, in contrast to the sharp

Table 1: Selected examples of frustrated magnetic materials

Short name	material	magnetic lattice size of moments	Spin model value of $\theta_{\rm CW}$
SCGO	$SrCr_{9-x}Ga_{3+x}O_9$	pyrochlore slabs $S = 3/2$	Heisenberg $\theta_{\rm CW} \approx -500K$
Spin ice	$Ho_2Ti_2O_7$ $Dy_2Ti_2O_7$	pyrochlore	Ising $\theta_{\rm CW} \approx +1.9K$
herbertsmithite	$ZnCu_3(OH)_6Cl_2$	kagome $S = 1/2$	Heisenberg $\theta_{\rm CW} \approx -300K$
κ-ET	$\kappa-(BEDT\text{-}TTF)_2Cu_2(CN)_3$	triangular $S = 1/2$	Heisenberg $\theta_{\rm CW} \approx -400K$

response from magnon excitations in an ordered magnet, single-crystal inelastic neutron scattering from herbertsmithite has structure broad in wavevector at all energies [10], as expected if the energy and momentum imparted by scattered neutrons are shared between multiple fractionalised excitations. Information on excitations can also be inferred from the dependence on temperature T of the heat capacity $C_{\rm p}$, which in κ-ET at low temperature fits the form $C_{\rm p} = \gamma T + \beta T^3$ [11]. While such behaviour is familiar in a metal, a contribution linear in T is remarkable in an insulator, suggesting formation of a spinon Fermi surface in a system that does not have mobile charges.

1.2 Classical ground state degeneracy

A first step in the discussion of classical frustrated magnets is to understand ground-state degeneracy. The character of this problem is different according to whether we treat discrete (e.g. Ising) or continuous (e.g. classical Heisenberg) spin variables, since we should count discrete ground states for the former, and continuous degrees of freedom within the ground-state manifold for the latter. In either case, a signature of a highly frustrated system is that the number we obtain in this way is extensive, suggesting that within ground states there are local fluctuations which take place independently in different parts of a large sample.

For the discrete case, an illustrative example is provided by the nearest neighbour Ising antiferromagnet on the pyrochlore lattice. Here an approximate but remarkably accurate estimate was provided by Pauling in the context of water ice [12] (see Section 4 for details of the link between water ice, spin ice, and the Ising antiferromagnet). As a start, note for a single tetrahedron that six states from a total of sixteen are ground states. A pyrochlore Ising model consisting of $N_{\rm T}$ tetrahedra contains $N_{\rm S} = 2N_{\rm T}$ spins, since there are four spins per tetrahedron but each spin is shared between two tetrahedra. It therefore has $2^{2N_{\rm T}}$ states in total. Treating the restriction to ground states as if it were independent on each tetrahedron, the number of ground states for the entire system is then estimated to be

$$2^{2N_{\rm T}} \times \left(\frac{6}{16}\right)^{N_{\rm T}} = \left(\frac{3}{2}\right)^{N_{\rm T}} = \left(\frac{3}{2}\right)^{N_{\rm S}/2} \tag{4}$$

and from this the ground-state entropy per spin is $\frac{k_{\rm B}}{2}\ln(3/2)$. Measurements of the low-temperature entropy in spin ice, obtained from the magnetic contribution to the heat capacity, are in striking agreement with this estimate [13].

For models with spins that can be rotated continuously, ground-state degrees of freedom are the ones remaining after respecting all ground state constraints. We can estimate their number D using an approach initiated in the context of mechanical systems by Maxwell [14, 15, 16]. Consider $N_{\rm S}$ classical n-component unit spins, constituting $F = N_{\rm S}(n-1)$ degrees of freedom. Suppose that these spins form a lattice of $N_{\rm C}$ corner-sharing, antiferromagnetically coupled, q-site clusters $\{\alpha\}$. Each cluster can be treated as in Eq. (1), and $N_{\rm S} = qN_{\rm C}/2$. Energy is minimised if the total magnetisation $\mathbf{L}_\alpha$ of every cluster is zero: a set of $K = nN_{\rm C}$ scalar constraints. If these constraints can be satisfied simultaneously and are linearly independent, we have

$$D = F - K = \left[\frac{q}{2}(n-1) - n\right] N_{\rm C}\,. \tag{5}$$

As an example, for Heisenberg spins ($n = 3$) on the pyrochlore lattice ($q = 4$) we get in this way the extensive result $F = N_{\rm C}$.

1.3 Order by disorder

Extensive ground-state degeneracy, in either the discrete or the continuous sense, is characteristic of many highly frustrated systems and offers a potential route to understanding suppression of order. However, not being symmetry-protected, this degeneracy may be lifted by fluctuations, a phenomenon termed *order by disorder* [17, 18].

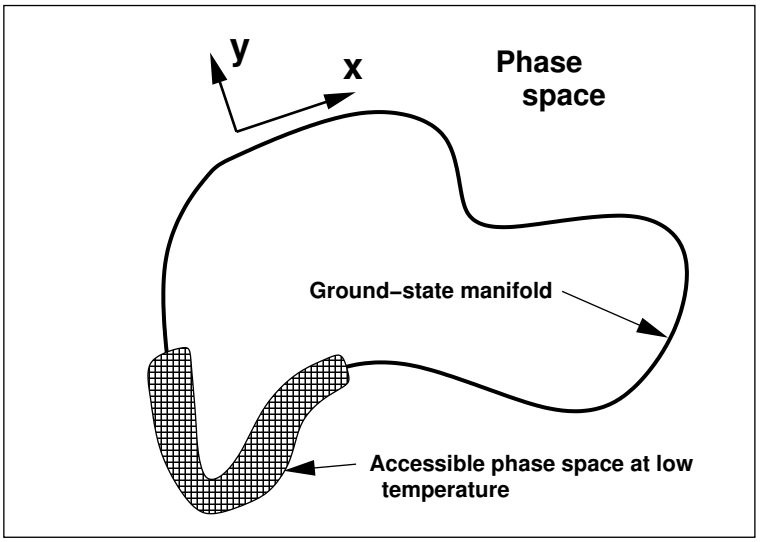

Figure 3: Schematic view of phase space for a geometrically frustrated magnet: the ground state manifold forms a high-dimensional subspace, and states accessible at low temperatures (partly marked by shading) lie close to it. Coordinates in phase space can be separated locally into ones ($\mathbf{x}$) within the ground-state subspace and others ($\mathbf{y}$) orthogonal to it.

The issues at stake are illustrated schematically in Fig. 3, where we consider in phase space the configurations that are accessible at low temperature and lie close to the ground state. Introducing coordinates $\mathbf{x}$ on the ground-state manifold and $\mathbf{y}$, locally orthogonal to it, by integrating out small amplitude fluctuations in $\mathbf{y}$, from an energy $\mathcal{H}(\mathbf{x},\mathbf{y})$ at inverse temperature β one induces a probability distribution on the ground state of the form (before normalisation)

$$\mathcal{Z}(\mathbf{x}) = \int \mathcal{D}\mathbf{y}\, e^{-\beta\mathcal{H}(\mathbf{x},\mathbf{y})} \propto \prod_k \frac{k_{\rm B}T}{\omega_k(\mathbf{x})}\,, \tag{6}$$

where the right-hand expression follows from a harmonic approximation for the dependence of $\mathcal{H}(\mathbf{x},\mathbf{y})$ on $\mathbf{y}$, under the assumption that the components of $\mathbf{y}$ consist of canonically conjugate pairs of generalised coordinates and momenta. Two alternatives now arise: this probability distribution may either represent a system that accesses all ground states at low temperature, or the probability density may be concentrated on a subset of ground states. For the latter, the states selected by fluctuations are ones with $\prod_k \omega_k(\mathbf{x})$ small. In practice these are likely to be states that are ordered in some way, in which a subset of $\omega_k(\mathbf{x})$ vanish.

This point can be illustrated by a toy calculation for four antiferromagnetically coupled classical XY ($n = 2$) or Heisenberg ($n = 3$) spins, with (1) as the Hamiltonian. The existence of a soft mode for special ground states in which all four spins are collinear is demonstrated in Fig. 4. To examine the consequences of this soft mode, consider at inverse temperature β the thermal distribution $P(\theta)$ of the angle θ between a pair of these spins, defined via $\cos\theta = \mathbf{S}_1 \cdot \mathbf{S}_2$. Let

$$\mathcal{Z}(\theta) = \int {\rm d}\mathbf{S}_3 {\rm d}\mathbf{S}_4\, e^{-\beta\mathcal{H}}\,. \tag{7}$$

Taking into account the volume factors of $\mathrm{d}\theta$ and $\sin\theta\mathrm{d}\theta$ for $n = 2$ and $n = 3$ respectively, one has $P(\theta)\mathrm{d}\theta \propto \mathcal{Z}(\theta)\mathrm{d}\theta$ for $n = 2$ and $P(\theta)\mathrm{d}\theta \propto \mathcal{Z}(\theta)\sin\theta\,\mathrm{d}\theta$ for $n = 3$. It is straightforward to evaluate $\mathcal{Z}(\theta)$ at large β and so obtain

$$P(\theta) \propto \left\{ \begin{array}{ll} (\sin\theta)^{-1} & \mathrm{XY} \\ \sin\theta/2 & \mathrm{Heisenberg} \end{array} \right. \tag{8}$$

The non-integrable divergences of $P(\theta)$ at θ=0 and θ=π for XY spins (which are rounded at finite β) indicates

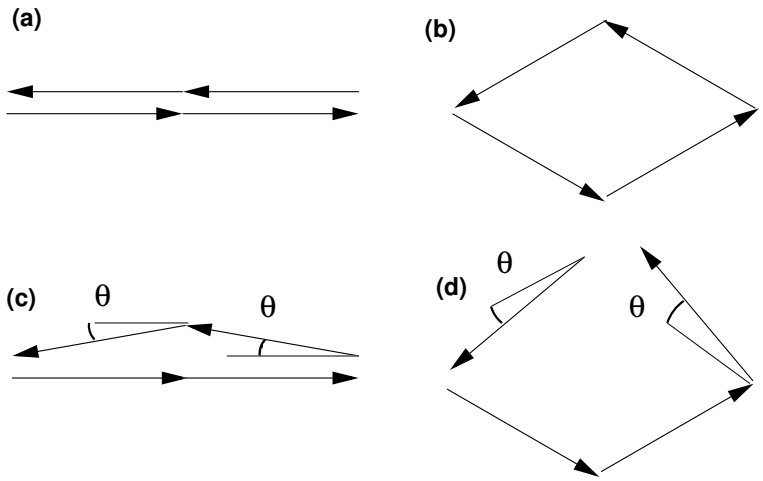

Figure 4: An illustration of how soft modes arise in selected ground states. Consider two ground states, (a) and (b), for four antiferromagnetically coupled spins, and two states (c) and (d), obtained by rotating pairs of spins through small angles θ. The total magnetisation varies differently with θ in the two cases. It is $\mathbf{L} \propto \theta^2$ in the example based on a collinear ground state, but $\mathbf{L} \propto \theta$ in the generic case. The energy cost of the excitation is hence $\mathcal{H} \propto \theta^4$ in the collinear case, but is generically $\mathcal{H} \propto \theta^2$.

that fluctuations select collinear spin configurations in the low-temperature limit. Conversely, Heisenberg spins sample all orientations even at arbitrarily temperature.

Moving from this toy problem to an extended lattice, there exists a catalogue of well-studied examples and a criterion for whether there is fluctuation-induced order. Instances of classical order-by-disorder include the kagome Heisenberg antiferromagnet (where co-planar spin configurations are selected [19]) and the pyrochlore XY antiferromagnet (with collinear order [16]), while a converse case is the pyrochlore Heisenberg antiferromagnet, which is thermally disordered at all temperatures [16]. A sufficient condition for order is that the ground-state probability distribution $\mathcal{Z}(\mathbf{x})$ has non-integrable divergences in the vicinity of the subset of configurations favoured by fluctuations, and one can assess whether that is the case by comparing the dimensionality of the full ground-state manifold with that of the soft subspace. For n-component spins on a lattice of corner-sharing clusters of q sites, order is expected if $n < (q+2)/(q-2)$ [16].

In Monte Carlo simulations of models with continuous degrees of freedom, the value of the low-temperature heat capacity C per spin provides a diagnostic for the presence of soft modes. A simple generalisation of the equipartition principle shows that a dependence of energy $\mathcal{H}$ on mode coordinate θ with the form $\mathcal{H} \propto |\theta|^n$ implies a contribution to C from this mode of $k_{\rm b}/n$. By this argument, one expects for unfrustrated classical Heisenberg models (with two degrees of freedom per spin) the value $C = k_{\rm B}$ at low temperature. In contrast, for the pyrochlore Heisenberg antiferromagnet, from Eq. (5) $1/4$ of modes cost no energy. The remaining modes are conventional, with an energy cost quadratic in displacement, and so $C = 3k_{\rm B}/4$ [16]. For the kagome Heisenberg antiferromagnet, one sixth of the fluctuation modes from a co-planar ground state cost an energy quartic in displacement, while the remainder are quadratic, so that $C = 11k_{\rm B}/12$ [19].

Quantum order by disorder depends on different features of the fluctuation spectrum from its thermal counterpart. In the notation of Eq. (6), the zero-point energy of quantum fluctuations out of the classical ground-state manifold generates an effective Hamiltonian

$$\mathcal{H}_{\rm eff}(\mathbf{x}) = \frac{1}{2}\sum_k \hbar\omega_k(\mathbf{x})\,. \tag{9}$$

Suppose $\mathcal{H}_{\rm eff}(\mathbf{x})$ has minima for preferred configurations $\mathbf{x} = \mathbf{x}_0$. There are quantum fluctuations of $\mathbf{x}$ about these configurations, because the set of ground state coordinates includes canonically conjugate pairs of generalised positions and momenta. At large spin S the amplitude of these fluctuations is small and one always expects order. Reducing S, we expect within this decription that a quantum-disordered ground state may emerge via delocalisation of the ground state wavefunction in the landscape $\mathcal{H}_{\rm eff}(\mathbf{x})$.

Experimental demonstrations of fluctuation-induced order rely on there being a good characterisation of interactions, so as to show that these do not drive ordering in a conventional way. For the garnet $Ca_3Fe_2Ge_3O_{12}$, a

material with two interpenetrating magnetic lattices coupled via zero-point fluctuations, it has been demonstrated that a spinwave gap in the Néel ordered state indeed arises mainly in this way, by independent determination of the size of single ion anisotropy (the other possible origin for the gap) [20], and via the characteristic temperature dependence of the gap [21]. In the context of highly frustrated systems, $Er_2Ti_2O_7$ has been thoroughly investigated as an example of a system with quantum order by disorder [22].

2 Classical spin liquids

The problem of finding a good description for the low-temperature states of classical frustrated magnets presents an obvious challenge. We would like to replace the high-energy spin degrees of freedom, which have strongly correlated fluctuations at low temperature, with a new set of low-energy degrees of freedom that are only weakly correlated. Remarkably, this turns out to be possible for some of the systems of most interest. Moreover, the emergent low-energy coordinates have simple and appealing interpretations, which we introduce in the following.

2.1 Simple approximations

As context for a discussion of low-temperature states in frustrated magnets, it is useful to examine what special features these systems present when treated them using some of the standard approximations. In particular, it is worthwhile to see how in some cases the absence of ordering is signalled within mean-field theory, and how an alternative approach known as the self-consistent Gaussian or large-n approximation can often give a good description of low-temperature correlations.

Recall the essentials of mean-field theory: thermal averages $\langle \ldots \rangle$ with respect to the full Hamiltonian $\mathcal{H}$ are approximated by averages $\langle \ldots \rangle_0$ using a tractable Hamiltonian $\mathcal{H}_0$. This gives a variational bound

$$\mathcal{F} \leq \langle \mathcal{H} \rangle_0 - T\mathcal{S}_0 \tag{10}$$

on the free energy $\mathcal{F}$ of the system, in terms of the energy $\langle \mathcal{H} \rangle_0$ and entropy $\mathcal{S}_0$ computed from $\mathcal{H}_0$. Taking a single-site $\mathcal{H}_0$, these quantities are parameterised by the site magnetisations $\{m_i\}$, leading to an expansion of the form

$$\langle \mathcal{H} \rangle_0 - TS_0 = \text{const.} + \sum_{\langle ij \rangle} J_{ij}\, m_i\, m_j + \frac{n}{2} k_{\mathrm{B}} T \sum_i m_i^2 + \mathcal{O}(m_i^4)\,, \tag{11}$$

with exchange interactions J_{ij}, where n is the number of spin components. Choosing the $\{m_i\}$ to minimise this estimate for F, one finds solutions of two types, depending on temperature: above the mean-field ordering temperature T_c, all $m_i = 0$, while for $T < T_c$ some $m_i \neq 0$. Within the mean field approximation, the value of T_c and the ordering pattern below T_c are determined from the eigenvalues and eigenvectors of the matrix J_{ij}: denoting the minimum eigenvalue (which is negative) by $\varepsilon_{\min}$ and an associated eigenvector by φ_i, one has $\varepsilon_{\min} + \frac{n}{2} k_{\mathrm{B}} T_c = 0$ and $m_i \propto \varphi_i$ for $T \lesssim T_c$. The distinction that arises in this framework between unfrustrated and highly frustrated systems concerns the degeneracy of $\varepsilon_{\min}$. In a conventional system the minimum eigenvalues form a discrete set. For example, in a nearest-neighbour square-lattice antiferromagnet the eigenvalues of the interaction matrix, labelled by a wavevector $\mathbf{q}$, are $J(\mathbf{q}) = J(\cos q_x + \cos q_y)$, and so $\varepsilon_{\min} = -2J$ at $\mathbf{q} = (\pi, \pi)$. By contrast, a number of important examples of highly frustrated magnets lead to minima of J_{ij} at all wavevectors, forming dispersionless or 'flat' bands across the Brillouin zone. Mean field theory fails for these systems by wrongly predicting ordering at a temperature $T_c \sim |\theta_{\mathrm{CW}}|$. A warning of this failure is provided by there being macroscopically many possible ordering patterns φ_i.

The appearance of flat bands with nearest neighbour interactions J on lattices built from corner-sharing clusters of q sites can be understood via the same Maxwell-counting approach that we employed in Eq. (5) to discuss ground-state degeneracy of systems such as the classical Heisenberg model on the same lattices. We start from the fact that $\varepsilon_{\min}$ is the minimum of $\sum_{ij} J_{ij}\varphi_i\varphi_j$ subject to the constraint $\sum_i \varphi_i^2 = 1$. For corner-sharing clusters, using i, j as site labels and α as a cluster label, we have

$$\sum_{ij} J_{ij}\varphi_i\varphi_j = J \sum_{\alpha} \Big| \sum_{i \in \alpha} \varphi_i \Big|^2 + \text{const.} \tag{12}$$

Eigenvectors associated with $\varepsilon_{\min}$ therefore satisfy $\sum_{i\in\alpha} \varphi_i = 0$ for all α. Using the notation of Eq. (5), these conditions amount to $K = N_{\mathrm{C}}$ constraints on the $F = N_{\mathrm{S}} = \frac{q}{2} N_{\mathrm{C}}$ degrees of freedom $\{\varphi_i\}$. Omitting sub-extensive terms, the degeneracy of $\varepsilon_{\min}$ is therefore

$$D = F - K = \Big(\frac{q}{2} - 1\Big) N_{\mathrm{C}}\,. \tag{13}$$

For example, on the kagome lattice one third of eigenvectors have eigenvalue $\varepsilon_{\rm min}$; as there are three sites in the unit cell, the matrix J_{ij} has three bands, of which the lowest is flat. Similarly, for the pyrochlore lattice there are four bands, of which the lowest two are degenerate and flat.

A successful treatment of these systems at low temperature must involve an average over correlated low-energy states. The self-consistent Gaussian approach provides a simple way of approximating this average and is widely applicable to systems in which all sites are symmetry-equivalent. The central idea is to replace an average over orientations of classical, fixed-length spins by independent Gaussian averages over the magnitudes of each component, with a variance chosen to maintain the correct spin length on average. These simplifications are exact in the limit that the number n of spin components is large, and in many instances they are remarkably accurate for $n = 3$ or even for $n = 1$ [23, 24]. Under this approximation the trace over spin configurations is written

$$\prod_i \int {\rm d}\mathbf{S}_i \ldots \delta(|\mathbf{S}_i| - 1) \approx \prod_i \int {\rm d}\mathbf{S}_i \ldots e^{-\frac{\lambda}{2}|\mathbf{S}_i|^2} \tag{14}$$

with the Lagrange multiplier λ determined by the condition $\langle |\mathbf{S}_i|^2 \rangle = 1$. Denoting the partition function by $\mathcal{Z}$, a general thermal average then takes the form

$$\langle \ldots \rangle = \mathcal{Z}^{-1} \int {\rm d}\{\mathbf{S}_i\} \ldots e^{-\frac{1}{2}\sum_{ij} \mathbf{S}_i(\beta J_{ij} + \lambda \delta_{ij})\mathbf{S}_j} \, . \tag{15}$$

In particular, the spin correlator is

$$\langle \mathbf{S}_i \cdot \mathbf{S}_j \rangle = n \left[(\beta {\rm J} + \lambda)^{-1} \right]_{ij} \tag{16}$$

and λ satisfies

$$n \left[(\beta {\rm J} + \lambda)^{-1} \right]_{ii} \equiv \frac{n}{N_{\rm S}} {\rm Tr} \frac{1}{(\beta {\rm J} + \lambda)} = 1 \, . \tag{17}$$

If the minimum eigenvalues of J form a flat band, then in the low-temperature limit $(\beta {\rm J} + \lambda)^{-1}$ is proportional to the projector $\mathbb{P}$ onto this band, so that $\langle \mathbf{S}_i \cdot \mathbf{S}_j \rangle \propto \mathbb{P}_{ij}$. In many of the systems we are concerned with (those with a Coulomb phase: see Sec. 4.2), $\mathbb{P}_{ij}$ falls off at large separation r_{ij} as $\mathbb{P}_{ij} \sim r_{ij}^{-d}$, where d is the spatial dimension.

2.2 The triangular lattice Ising antiferromagnet and height models

Moving beyond these simple approximations, we would like to find a description of low-energy spin configurations that respects microscopic constraints imposed by the Hamiltonian but is amenable to coarse graining. An early and illuminating example is provided by a mapping which we now describe, from the triangular lattice Ising antiferromagnet to a height model.

As background, we note that this Ising model (probably the first highly frustrated magnet to be studied in detail [25]) has a macroscopically degenerate ground state, and ground-state spin correlations that are known from an exact solution to decay with distance as $r^{-1/2}$. In ground states every elementary triangle of the lattice has two spins parallel and one antiparallel. Degeneracy arises because many such configurations include some spins that are subject to zero net exchange field and can therefore be reversed at zero energy cost, as illustrated in Fig. 5 (left). To avoid confusion, we should point out that the degeneracy on this lattice is specific to the Ising model, and not a consequence of flat bands.

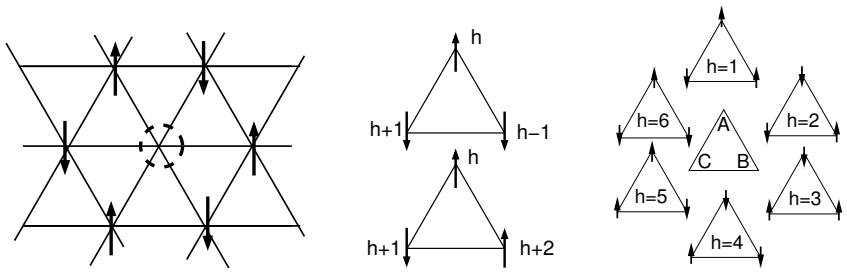

Figure 5: Triangular lattice Ising antiferromagnet spin configurations. Left: state with a flippable spin, marked with a circle. Centre: mapping from spins to heights at sites. Right: mapping from spin orientations on the three sublattices (marked A, B and C) to triangle heights in flat states.

Spin configurations can be mapped onto a new variable, termed a height field, in such a way that the ground-state condition in the spin model translates into a condition that the height field is single-valued. The mapping associates an integer height h_i with each site i [26, 27]. To describe it, we introduce a direction on each bond of the lattice in such a way that there is (say) anticlockwise circulation around 'up' triangles and clockwise circulation around 'down' triangles. With the height of an origin site chosen arbitrarily, the height change on traversing a bond in the positive direction is $+1$ if the bond links antiparallel (unfrustrated) spins, and -2 if it links parallel (frustrated) spins, as illustrated in Fig. 5 (centre). A convenient further stage is to define heights $h(\mathbf{r})$ at the centres of triangles that are averages of the three values at corners: see Fig. 5 (right).

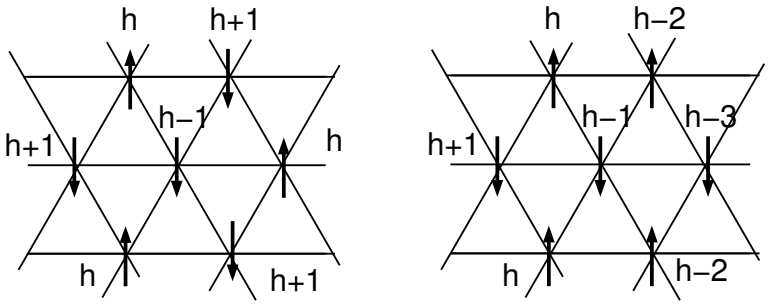

Figure 6: Triangular lattice Ising antiferromagnet spin configurations and mappings to height field. Left: state with flippable spin generating a flat height field (with the value h at all triangle centres). Right: spin state without flippable spins, that generates a height field with maximum gradient (heights at triangle centres decrease by 1 on going from any triangle to its right-hand neighbour).

As demonstrated with examples in Fig. 6, configurations with a flippable spin are locally flat, and those in which the gradient of the height field is maximal have no flippable spins. These facts motivate a coarse-grained theory in which $h(\mathbf{r})$ is taken to be a real-valued function of a continuous coordinate, with an entropic weight on configurations that (in the first approximation) has the form

$$P[h(\mathbf{r})] = \mathcal{Z}^{-1} e^{-\mathcal{H}} \tag{18}$$

where

$$\mathcal{H} = \frac{K}{2} \int \mathrm{d}^2\mathbf{r} |\nabla h(\mathbf{r})|^2 \tag{19}$$

and $\mathcal{Z}$ is the usual normalisation. The inverse mapping between spins and heights (modulo 6) is shown in Fig. 5 (right) for the six distinct flat states. It has the algebraic form

$$S(\mathbf{r}) \simeq \cos(\pi h(\mathbf{r})/3 + \varphi_\alpha), \tag{20}$$

where we have omitted higher Fourier components of $h(\mathbf{r})$, and the phase φ_α takes the values $0, \pm 2\pi/3$ depending on the sublattice α.

The height field $h(\mathbf{r})$ has fluctuations that diverge logarithmically with separation, as we see from an explicit calculation. For a system of size $L \times L$, define the Fourier transform

$$h_{\mathbf{q}} = \frac{1}{L} \int \mathrm{d}^2\mathbf{r}\, e^{i\mathbf{q}\cdot\mathbf{r}} h(\mathbf{r}) \qquad \text{so that} \qquad \mathcal{H} = \frac{K}{2} \sum_{\mathbf{q}} q^2 |h_{\mathbf{q}}|^2 \,.$$

Then, with short-distance cut-off a,

$$\begin{aligned} \langle [h(\mathbf{0}) - h(\mathbf{r})]^2 \rangle &= \frac{2}{L^2} \sum_{\mathbf{q}} (1 - \cos \mathbf{q}\cdot\mathbf{r}) \langle |h_{\mathbf{q}}|^2 \rangle \\ &= \frac{1}{2\pi^2} \int \mathrm{d}^2\mathbf{q}\, \frac{1 - \cos \mathbf{q}\cdot\mathbf{r}}{Kq^2} \\ &\simeq \frac{1}{\pi K} \ln(r/a) \,. \end{aligned} \tag{21}$$

Putting these ingredients together, we can evaluate the spin correlator using the coarse-grained theory. For two sites on the same sublattice we obtain

$$\langle \sigma(\mathbf{0})\sigma(\mathbf{r})\rangle \propto \langle e^{i\frac{\pi}{3}[h(\mathbf{0})-h(\mathbf{r})]}\rangle = e^{-\frac{\pi^2}{18}\langle [h(\mathbf{0})-h(\mathbf{r})]^2\rangle} = (r/a)^{-\pi/18K} . \tag{22}$$

The power-law form illustrates the consequences of large but strongly correlated ground-state fluctuations, and a comparison with exact results for the Ising model fixes the value of the height model stiffness as $K = \pi/9$.

The leading approximation that has been made in using the height model to represent the triangular lattice Ising antiferromagnet is to treat $h(\mathbf{r})$ as a real, rather than integer-valued field. To correct this we can consider the replacement $\mathcal{H} \to \mathcal{H} + \mathcal{H}_1$ with $\mathcal{H}_1 = -g \int \mathrm{d}^2\mathbf{r} \cos 2\pi h(\mathbf{r})$, so that values of $h(\mathbf{r})$ close to integers are preferred. One finds that $\mathcal{H}_1$ is an irrelevant perturbation at the renormalisation group fixed point represented by $\mathcal{H}$ if $K < \pi/2$, as is the case for the height model that represents the triangular lattice Ising antiferromagnet. Changes to the Ising model (for example, higher spin [27]) may increase K so that $\mathcal{H}_1$ is relevant. The height field than locks to a particular integer value, representing long-range order of the Ising spins.

Excitations out of the ground state have an attractively simple description in height-model language. From the rules of Fig. 5 we see that if the three Ising spins of an elementary triangle have the same orientation, the height field is no longer everywhere single-valued: it changes by ± 6 on encircling the triangle that carries the excitation. A single spin flip can introduce such excitations into a ground-state configuration only as vortex anti-vortex pairs, since a local move leaves the distant height field unchanged. A vortex and anti-vortex can be separated by additional spin flips without further increase in exchange energy, and constitute our first example of a fractionalised excitation.

Vortices are dilute at low temperature, because they have an energy cost $4J$. Their presence also changes the number of ground states available to the system, and so they have an entropy cost. This can be calculated within the height description. A vortex at the origin leads to an average height gradient at radius r of $|\nabla h(\mathbf{r})| = 6/(2\pi r)$. In a system of linear size L this generates a contribution to $\mathcal{H}$ of

$$\frac{K}{2}\int \mathrm{d}^2\mathbf{r}\, |\nabla h(\mathbf{r})|^2 = \frac{9K}{\pi}\ln(L/a) . \tag{23}$$

Similarly, the presence of a vortex anti-vortex pair at fixed positions with separation r has an entropy cost that depends on their separation. As a consequence, the pair is subject to an entropic attractive potential $V(r) \simeq \frac{9K}{\pi}\ln(r/a)$.

The entropy cost for vortices should be compared with the entropy gain $2\ln(L/a)$ arising from translations: vortex anti-vortex pairs are unbound if $9K/\pi < 2$, as is the case here. In the setting of the Ising model, this means that the power-law correlations of the ground state are cut off at non-zero temperature by a finite correlation length, set by the vortex separation. This correlation length is much larger than the lattice spacing if $T \ll J/k_{\mathrm{B}}$, and it diverges as $T \to 0$.

In summary, the triangular lattice Ising antiferromagnet provides an illustration of a system that, in its ground state, combines finite entropy with long-range correlations. The height model shows how these features can be captured in a long-wavelength description. The physics of the triangular lattice Ising antiferromagnet at low temperature, including power-law correlations and fractionalised excitations, has important generalisations to other systems, including most notably spin ice. In addition, some of the main theoretical tools used in a long-wavelength description of these generalised problems are extensions of the ones underlying the height model. Many of these ideas are exemplified in classical dimer models, which we now introduce.

3 Classical dimer models

Classical dimers models [28, 29, 30] offer a setting in which to discuss some general features of the statistical physics of systems that are both highly degenerate and strongly constrained. They are important in their own right and also serve as the foundation for a treatment of quantum spin liquids using quantum dimer models.

3.1 Introduction

The configurations of a dimer model are close-packed coverings of a lattice, with dimers arranged on bonds in such a way that there is, in the simplest case, exactly one dimer touching each lattice site. Examples are shown in Fig. 7. Entropy arises from rearrangements of dimers. Consider, in an initial covering, a closed loop of bonds that are alternately empty and occupied by dimers. The configuration on this loop can be flipped, exchanging empty and occupied bonds, independently of the configurations on other loops that do not intersect this one.

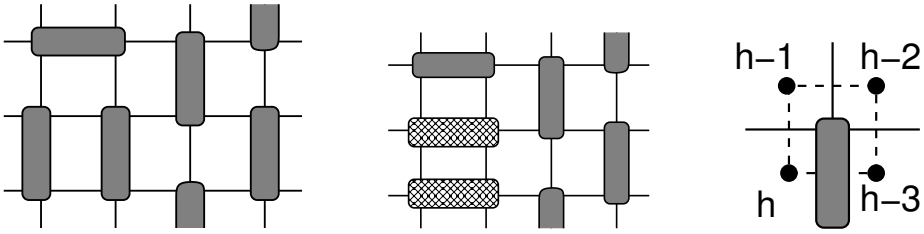

Figure 7: States of square lattice dimer model. Left: close-packed configuration. Centre: local rearrangement. Right: mapping to height model.

Close-packed dimer configurations on a planar lattice admit a height representation provided the lattice is bipartite. Let z be the coordination number of the lattice, and introduce the dual lattice, which has sites at the centres of the plaquettes of the original lattice, and links intersecting the edges of these plaquettes. The height field is defined at sites of the dual lattice: traversing in (say) an anti-clockwise direction the plaquettes of the dual lattice that enclose A-sublattice sites of the original lattice, we take the height difference to be $\Delta h = +1$ on crossing an empty bond, and $\Delta h = 1 - z$ on crossing the occupied bond, as in Fig. 7 (right). A simple generalisation is to take dimer configurations in which exactly n dimers touch each site. Then $\Delta h = +n$ for empty bonds and $n - z$ for occupied ones. These choices ensure that the height field is single-valued

There is in fact an exact correspondence between close-packed dimer configurations on the hexagonal lattice and ground states of the triangular lattice Ising antiferromagnet. To establish this, note that the hexagonal lattice has as its dual the triangular lattice. Under the correspondence, dimers on the hexagonal lattice lie across frustrated bonds of the triangular lattice, as in Fig. 8. In a ground state of the Ising model, the exchange interaction on exactly one edge of every elementary triangle is frustrated, and so in the corresponding dimer covering, every site of the hexagonal lattice is touched by exactly one dimer.

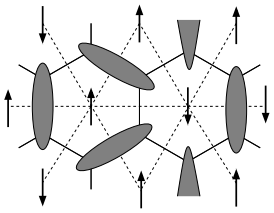

Figure 8: The hexagonal lattice dimer model and its correspondence with ground states of triangular lattice Ising antiferromagnet.

3.2 General formulation

While the mapping from dimer coverings to a height field is particular to two-dimensional, bipartite lattices, it can be reformulated in language that generalises directly to higher dimensions [31]. To do so, we first make use of the bipartite nature of the lattice to define an orientation convention on nearest neighbour bonds, taking the direction to be from (say) the A-sublattice to the B-sublattice. We then define for each dimer configuration a flux in this direction on each link, which (for a lattice with coordination number z) is $1 - z$ on links occupied by a dimer, and $+1$ on unoccupied links.

This flux is constrained by its construction to be divergenceless for a dimer covering that everywhere obeys the rule of exactly one dimer meeting each site. The constraint can be resolved in the usual way, by taking the flux to be the curl of a vector potential $\vec{A}(\mathbf{r})$. In the continuum this is of course familiar for a three-dimensional system. It also applies to a two-dimensional system: one takes $\vec{A}(\mathbf{r}) = \hat{z}h(x, y)$, with $\hat{z}$ the normal to the plane of the system and $h(x, y)$ a scalar, which we will see is simply the height field.

The next step is to write a coarse-grained free energy for dimer configurations that generalises the height model. In three dimensions as in two, coarse-grained states with high entropy arise from configurations in which there are many short loops of bonds alternately occupied and unoccupied by dimers, around which dimer occupations can be flipped. Those loops correspond roughly to closed flux lines: flux has a constant direction around each loop,

although its magnitude alternates between occupied and unoccupied bonds. Configurations containing mainly small closed flux loops generate small values of coarse-grained flux, and conversely there is an entropy penalty attached to large flux. This motivates the conjecture [31]

$$\mathcal{H} = \frac{K}{2} \int \mathrm{d}^3\mathbf{r}\, |\vec{\nabla} \times \vec{A}(\mathbf{r})|^2 \,. \tag{24}$$

as a generalisation of Eq. (19), from which the height model is recovered in two dimensions via the substitution $\vec{A}(\mathbf{r}) = \hat{z}h(x, y)$.

Despite the equivalent forms of $\mathcal{H}$ in two and three dimensions, there are important differences. For the two-dimensional model, the value of the stiffness K determines the location of the theory on a line of fixed points and controls which possible perturbations are RG-relevant. By contrast, for the three-dimensional model there are no symmetry-allowed perturbations that are RG-relevant, and the value of K simply sets the amplitude of fluctuations.

Dimer correlations can be evaluated straightforwardly since the theory is Gaussian. We introduce a dimer number operator $\sigma_{\hat{\tau}}(\mathbf{r})$, which takes the value $\sigma_{\hat{\tau}}(\mathbf{r}) = +1$ if the bond in direction $\hat{\tau}$ centred at $\mathbf{r}$ is occupied by a dimer, and otherwise has the value $\sigma_{\hat{\tau}}(\mathbf{r}) = -1$. Defining the flux density $\vec{B}(\mathbf{r}) = \vec{\nabla} \times \vec{A}(\mathbf{r})$, the connected dimer density correlation function is

$$C_{kl}(\mathbf{r}_1, \mathbf{r}_2) \equiv \langle \sigma_{\hat{k}}(\mathbf{r}_1)\sigma_{\hat{l}}(\mathbf{r}_2)\rangle - \langle \sigma_{\hat{k}}(\mathbf{r}_1)\rangle\langle \sigma_{\hat{l}}(\mathbf{r}_2)\rangle \propto \langle B^k(\mathbf{r}_1)B^l(\mathbf{r}_2)\rangle \,. \tag{25}$$

In two dimensions, $B^i(\mathbf{r}) = \epsilon_{ij}\partial_j h(\mathbf{r})$ and we can compute $\langle B^i(\mathbf{0})B^j(\mathbf{r})\rangle$ by differentiating Eq. (21), with the result

$$\langle B^i(0)B^j(\mathbf{r})\rangle = \frac{1}{2\pi K} \frac{2x_i x_j - \delta_{ij} r^2}{r^4} \,. \tag{26}$$

Similarly, in three dimensions, defining Fourier transforms in a system of linear size L via

$$\vec{B}_{\mathbf{q}} = L^{-3/2} \int \mathrm{d}^3\mathbf{r}\, e^{i\mathbf{q}\cdot\mathbf{r}} \vec{B}(\mathbf{r}) \qquad \text{and} \qquad \vec{B}(\mathbf{r}) = L^{-3/2} \sum_{\mathbf{q}} e^{-i\mathbf{q}\cdot\mathbf{r}} \vec{B}_{\mathbf{q}} \,, \tag{27}$$

one finds

$$\langle B^i_{\mathbf{q}} B^j_{\mathbf{k}}\rangle = \frac{1}{K} \left(\delta_{ij} - \frac{q_i q_j}{q^2} \right) \delta_{\mathbf{q},-\mathbf{k}} \tag{28}$$

and hence [31]

$$\langle B^i(0)B^j(\mathbf{r})\rangle = \frac{1}{4\pi K} \frac{3r_i r_j - \delta_{ij} r^2}{r^5} \,. \tag{29}$$

We see that, while dimer coverings of bipartite lattices described by this coarse-grained theory are disordered, with finite entropy density and no local symmetry breaking, the constraints of close packing and hard-core exclusion lead to power-law correlations with a characteristic form. States with these correlations are known as Coulomb phases [36].

3.3 Flux sectors, $U(1)$ and $\mathbb{Z}_2$ theories

It is an important feature of dimer models on bipartite lattices that the configuration space divides into sectors which are not connected by any local dimer rearrangements. For a system with periodic boundary conditions, these sectors are distinguished by the values of total flux encircling the system in each direction. Dimer rearrangements around short loops leave these global fluxes unchanged, and the order characterised by the fluxes is referred to as topological.

This definition of global flux is illustrated in Fig. 9. Let $N_\uparrow$ be the number of dimers that cross the line A-B on upward-directed links, and let $N_\downarrow$ be the number on downward-directed links. (In d dimensions, this line is replaced by a $(d-1)$-dimensional hypersurface.) Then the net flux across the line (or hypersurface) is $\Phi = z(N_\downarrow - N_\uparrow)$, where the coordination number is $z = 4$ for the square lattice. The value of Φ is unchanged by flipping dimers on contractable loops (ones that do not wrap around the system), as shown in Fig. 9 (ii) and (iii). Moreover, although microscopic values of the flux Φ are discrete, this restriction is unimportant after coarse-graining: for a three-dimensional system in the continuum limit we can view $\vec{A}(\mathbf{r})$ as the vector potential for a continuous-valued flux density $\vec{B}(\mathbf{r}) = \vec{\nabla} \times \vec{A}(\mathbf{r})$. Then Eq. (24) is simply the action for a U(1) gauge theory.

Dimer models can equally be defined on lattices that are not bipartite, but the long-distance physics in these cases is very different. For these systems it is not possible to define a local divergenceless flux, and sectors of configuration space are labelled by $\mathbb{Z}_2$ rather than U(1) quantum numbers. For a d-dimensional system there are d

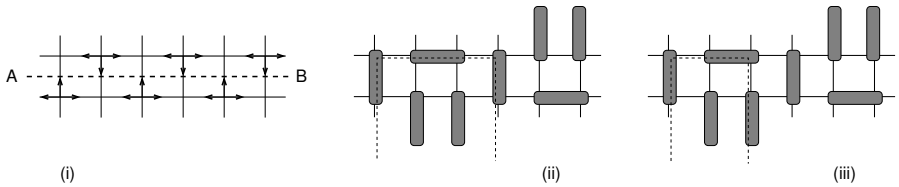

Figure 9: Flux sectors in a bipartite lattice dimer model. (i) Orientation convention on edges of the lattice. (ii) A dimer flip on the marked loop changes both $N_\uparrow$ and $N_\downarrow$ by 1. (iii) A dimer flip on a different marked loop changes local contributions to $N_\uparrow$ by ± 1 but leaves its net value unaltered.

of these quantum numbers, giving the parity of the number N of dimers intersecting a set of $(d-1)$-dimensional hypersurfaces. A change in the dimer configuration produced by flipping dimers on a contractable loop leaves these parities unchanged. To see this, note that the loop intersects the surface an even number of times, and consider the contribution to overall parity from two successive interactions. If the length of the loop between the crossings is even, then both intersections make the same contribution (both 0 or both 1) to N, and the combined contribution modulo 2 is unchanged when dimers on the loop are flipped; alternatively, if the length between crossings is odd, the two interactions make opposite contributions (one 0 and the other 1) to N, and their individual contributions swap when dimers are flipped.

It is known from exact solutions for two-dimensional lattices using Pfaffians [33], and from Monte Carlo simulations in three dimensions [31], that dimer-dimer correlations generically decay exponentially with separation for close-packed dimer coverings of non-bipartite lattices.

3.4 Excitations

Vortices in the height representation can arise from defects of more than one type in the dimer covering. One of these is obvious from the mapping between triangular lattice spin configurations and hexagonal lattice dimer configurations: a triangle in which three spins have the same orientation maps to a site of the hexagonal lattice at which three dimers meet. This excitation acts as a source or sink of the flux we have introduced, depending on which sublattice the site belongs to.

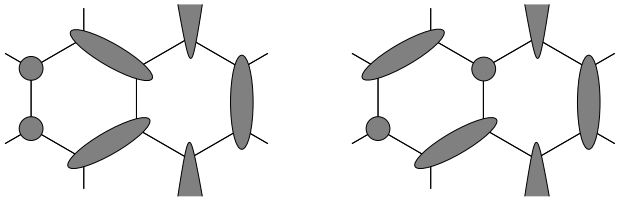

Figure 10: Monomers in the hexagonal lattice dimer model. Left: dimer replaced with two monomers. Right: separation of the monomers by dimer flips.

An alternative type of height vortex, which is of interest for the dimer model, is one in which a dimer is removed, or equivalently, replaced by two monomers, as in Fig. 10. The two monomers can be separated by subsequent dimer moves, one always remaining on the A-sublattice and the other on the B-sublattice. The two monomers are represented by a vortex anti-vortex pair in the height model. From the arguments leading to Eq. (23), we see that such a pair will be subject to an attractive entropic potential that increases logarithmically with separation.

This entropic potential is a natural consequence of the fact that a monomer acts as a source for flux $\vec{B}(\mathbf{r})$ if it is on one sublattice, and as a sink if it is on the other sublattice, and the logarithmic dependence on distance is characteristic of the Coulomb interaction in two dimensions. Similarly, the entropic potential $V(r)$ in three dimensions between a pair of monomers on opposite sublattices at separation r can be evaluated straightforwardly within the continuum description of Eq. (24). The presence of the excitations results in an additional contribution to $\vec{B}(\mathbf{r})$. Let $\vec{B}_{\rm source}$ be the field configuration that minimises $\mathcal{H}$ in the presence of the pair, and write $\vec{B}(\mathbf{r}) = \vec{B}_{\rm source} + \delta\vec{B}$. Since $\mathcal{H}$ is quadratic in $\vec{B}(\mathbf{r})$, integration over fluctuations $\delta\vec{B}$ yields a weight that is unaffected

by the presence or separation of the pair. We can therefore determine $V(r)$ simply from $\vec{B}_{\rm source}$, and by the usual arguments of electrostatics we find

$$V(r) = -\frac{K}{4\pi r}\,. \tag{30}$$

Since the entropic cost of separating the pair to infinity is bounded, monomer excitations in a Coulomb phase in three dimensions are deconfined.

In a dimer model that has long-range order, monomers are subject to a potential that grows much more rapidly with separation. For example, in two dimensions the coarse-grained height field steps between different pinned values along a line joining the vortex anti-vortex pair. This generates an interaction that is linear in separation, and the same result holds in three dimensions.

On non-bipartite lattices in both two and three dimensions the entropic interaction potential between a pair of monomers approaches a finite limiting value exponentially fast with increasing separation, provided the dimer coverings are disordered. The deconfinement of monomers is an important property distinguishing $\mathbb{Z}_2$ from U(1) phases in two dimensions.

It is characteristic of topologically ordered systems that transitions between ground states of a system on a torus can be engineered by a sequence of steps, consisting of the generation of a pair of excitations, followed by transport of one excitation around the torus, and ending with recombination. For a dimer model the first of these steps is the replacement of a dimer by a pair of monomers. The flux quantum number for the dimer covering is changed if one of these monomers is transported around the torus by flipping dimers, until the two monomers are again adjacent and can be replaced with a dimer.

4 Spin ice

The spin-ice materials $Ho_2Ti_2O_7$ and $Dy_2Ti_2O_7$ provide fascinating realisations of the Ising antiferromagnet on the pyrochlore lattice, in which both the nearest-neighbour and the long-range dipolar contributions to spin interactions make very distinctive contributions to the physical behaviour [34]. In this section we give an overview of the resulting physics, making use of some of the general ideas developed in our discussion of Coulomb phases.

4.1 Materials

Isolated Ho^{3+} and Dy^{3+} ions have high angular momentum ($J = 8$ and $J = 15/2$ respectively) and large magnetic moments ($10\mu_{\rm B}$ in both cases). In spin-ice materials the effect of the electrostatic environment of the rare earth ions is to split the $2J + 1$ degenerate states of the free ions into crystal field levels. Approximating the crystal field Hamiltonian by $-D(J_z)^2$, one has for positive D a ground state doublet $M_J = \pm J$. Since excited crystal field levels are several hundred kelvin higher in energy and the scale for interactions between spins is only a few kelvin, the moments can be represented by Ising pseudospins S_i. The easy axis at given a site is the local $\langle 111\rangle$ direction joining the centres of the two tetrahedra that share it, and so moments are directed either into or out of tetrahedra, as shown in Fig. 11. The centres of tetrahedra of the pyrochlore lattice lie on a diamond lattice, which is bipartite. We take the convention that $S_i = +1$ represents a spin directed out of a tetrahedron on the A-sublattice.

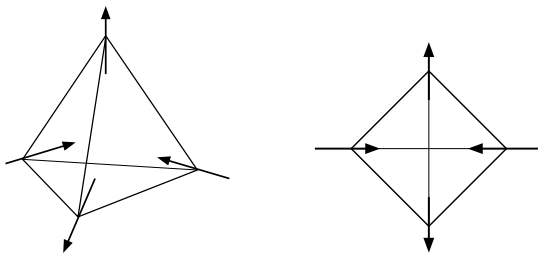

Figure 11: Magnetic moments at sites of a pyrochlore lattice, orientated along local $\langle 111\rangle$ axes in a 'two-in two-out' state. In later figures, for ease of drawing, we represent the tetrahedron in the flattened way shown on the right.

Strikingly, frustration arises from the combination of this local easy-axis anisotropy with *ferromagnetic* nearest-neighbour coupling ($\theta_{\rm CW} \simeq +1.9$K and $+0.5$K for the Ho and Dy compounds, respectively), and energy is

minimised for the two-in two-out states of the type illustrated in Fig. 11 [35]. The term *spin ice* is chosen because these spin arrangements mimic the proton positions in water-ice. As the values of $\theta_{\rm CW}$ are relatively small and the magnetic moments are large, long-range dipolar interactions are important in addition to the nearest neighbour coupling; we discuss their consequences in Sec. 4.3, but first examine the physics of the nearest-neighbour model.

4.2 Coulomb phase correlations

We would like to develop a description of ground states of the nearest-neighbour model for spin ice that is analogous to the height representation for the triangular lattice Ising antiferromagnet, and amenable to coarse-graining. The approach [24, 36] parallels the one introduced for three-dimensional dimer models in Sec. 3

In order to describe in a general way the ideas that are involved, it is useful to introduce some terminology. For a given system of corner-sharing frustrated clusters, we will be concerned with two types of lattice. One is simply the magnetic lattice on which the moments reside, also known as the medial lattice, and we denote this by $\mathcal{L}$. The other is the cluster (or simplex) lattice, also known as the pre-medial or parent lattice, which we denote by $\mathcal{B}$. The sites of $\mathcal{L}$ lie at the midpoints of the links of $\mathcal{B}$, and in the notation of graph theory, $\mathcal{L}$ is the line graph associated with the graph $\mathcal{B}$. For spin ice, $\mathcal{L}$ is the pyrochlore lattice and $\mathcal{B}$ is the diamond lattice. Alternatively, if we take $\mathcal{L}$ to be the kagome lattice, then $\mathcal{B}$ is the hexagonal lattice.

A key requirement in the following is that $\mathcal{B}$ should be a bipartite lattice. We can then orient the links of $\mathcal{B}$, say from sites of sublattice A to sites of sublattice B. Let $\hat{e}_i$ be the unit vector in this direction on link i, and note that i also labels a site of $\mathcal{L}$.

The central idea is to introduce a vector field $\vec{B}$, defined on the links of $\mathcal{B}$, that is a representation of a configuration of Ising spins $\{S_i\}$ on $\mathcal{L}$, and given by the relation

$$\vec{B}_i = S_i \hat{e}_i \,. \tag{31}$$

The field $\vec{B}$ is a useful construction because the ground-state condition for spin ice – that two spins are directed into each tetrahedron, and two are directed out – translates into the condition that $\vec{B}$ has zero lattice divergence at each node of $\mathcal{B}$. The field $\vec{B}$ is therefore an emergent gauge field.

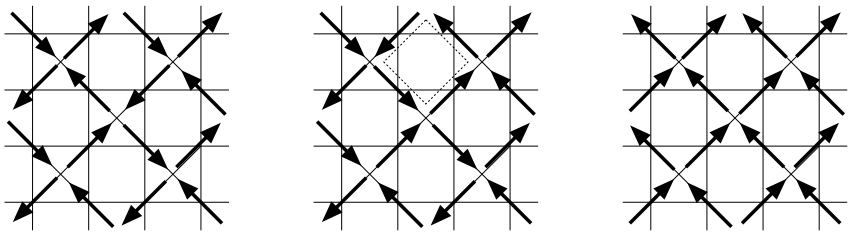

Figure 12: Ground-state configurations on the two-dimensional pyrochlore lattice. Left: a state containing short flippable loops of spins. Centre: the state obtained from this by flipping four spins on the marked loop. Right: a state with no flippable spins and maximal flux $\vec{B}$.

The next step is to conjecture a probability distribution for a coarse-grained version of $\vec{B}$. Some ground states contain short loops of flippable spins: closed loops on the $\mathcal{B}$ lattice, around which all spins are directed in the same sense. Further ground states with a similar coarse-grained $\vec{B}$ are obtained by reversing all the spins on one of these loops, and so entropy favours states with a high density of short loops, as illustrated in Fig. 12 using a two-dimensional version of the pyrochlore lattice. These considerations suggest that states in which $\vec{B}$ is large have lower entropy. This motivates for the probability distribution the form

$$P[\vec{B}(\mathbf{r})] = \mathcal{Z}^{-1} e^{-\mathcal{H}} \tag{32}$$

with

$$\mathcal{H} = \frac{K}{2} \int \mathrm{d}^3\mathbf{r} |\vec{B}(\mathbf{r})|^2 \,, \tag{33}$$

where $\vec{B}(\mathbf{r})$ is a continuum field, subject to the ground-state constraint $\vec{\nabla}\cdot\vec{B} = 0$, just as in our earlier discussion of Coulomb phases in dimer models. Indeed, spin ice ground states can be represented directly by dimer coverings on the diamond lattice with two dimers touching every site, simply by using dimers on $\mathcal{B}$ to represent spins $S_i = +1$ on $\mathcal{L}$. Ground state spin correlations in spin ice therefore have the dipolar form given in Eq. (29).

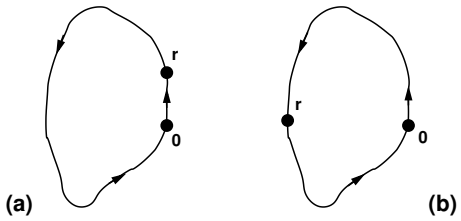

Figure 13: Illustration of the origin of dipolar correlations in spin ice. Spins at 0 and $\mathbf{r}$ are correlated if a flux line of the emergent field $\vec{B}(\mathbf{r})$ passes through both sites. The orientations of the flux line at the two sites depends on the direction of their spatial separation, so that for (a) $\langle S_0 S_{\mathbf{r}} \rangle > 0$ and for (b) $\langle S_0 S_{\mathbf{r}} \rangle < 0$.

The angular dependence of this correlator means that a pair of well-separated spins on sites of the same sublattice of $\mathcal{L}$ (and hence with the same orientation for $\hat{e}$ at both sites) are positively correlated if their separation vector $\mathbf{r}$ is in the direction of $\hat{e}$, but most likely to be anti-aligned if $\mathbf{r}$ is perpendicular to $\hat{e}$. Such behaviour can be understood by considering the geometry of flux lines of the emergent gauge field $\vec{B}(\mathbf{r})$. A spin configuration in which $\sigma_0 = +1$ is one with a flux line passing through the origin in the direction $\hat{e}$, and this flux line must close on itself since the field is divergenceless. The spin $\sigma_{\mathbf{r}}$ is correlated with σ_0 only in those configurations in which the same flux line passes through $\mathbf{r}$, and the most likely orientation of this flux line at $\mathbf{r}$ depends on the relative directions of $\mathbf{r}$ and $\hat{e}$, as shown in Fig. 13. The reciprocal space signature, Eq. (28), of these correlations consists of so-called pinch-point structures, sharp but without divergences, observed in elastic neutron diffraction [9].

It is interesting to connect the results obtained from a continuum treatment of the emergent gauge field to those arising from the self-consistent Gaussian approximation of Section 2.1. Adopting the sublattice labels and axis orientations shown in Fig. 14, the net Ising moment M and flux components B_x, B_y and B_z arising from a spin configuration S_1, S_2, S_3 and S_4 on the four sublattices are [37]

$$\begin{pmatrix} M \\ B_x \\ B_y \\ B_z \end{pmatrix} = \frac{1}{2} \begin{pmatrix} 1 & 1 & 1 & 1 \\ 1 & 1 & -1 & -1 \\ 1 & -1 & 1 & -1 \\ 1 & -1 & -1 & 1 \end{pmatrix} \cdot \begin{pmatrix} S_1 \\ S_2 \\ S_3 \\ S_4 \end{pmatrix} . \tag{34}$$

The statistical weight of fluctuations is determined within the self-consistent Gaussian approximation by their energy and by a Lagrange multiplier λ. From Eq. 1, the energy per unit cell of a configuration is $\frac{J}{2} M^2$. Moreover, the net Ising moment M is simply the lattice version of $\vec{\nabla} \cdot \vec{B}$. In continuum notation, Eq. 15 therefore amounts to a Boltzmann factor $e^{-\mathcal{H}}$ with

$$\mathcal{H} = \int \mathrm{d}^3 \mathbf{r} \left\{ \frac{\lambda}{2} |\vec{B}(\mathbf{r})|^2 + \frac{\beta J}{2} M^2 \right\} . \tag{35}$$

In this way we see that λ sets the value of the stiffness K for fluctuations of $\vec{B}(\mathbf{r})$. We also recover the condition $\vec{\nabla} \cdot \vec{B}(\mathbf{r}) = 0$ in the low-temperature limit $\beta J \to \infty$.

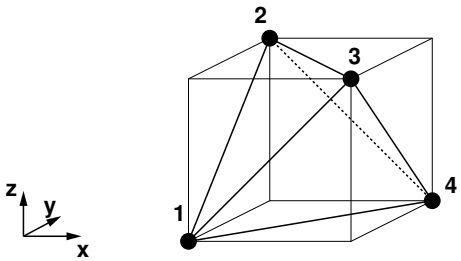

Figure 14: Choice of axes and sublattice labels for the pyrochlore lattice.

4.3 Monopoles

Some beautiful physics becomes apparent when we examine configurations of spin ice that do not obey the two-in two-out rule for ground states of the model with nearest neighbour interactions [38]. Consider the configuration

obtained from a ground state by reversing a single spin. As illustrated in Fig. 15, two separate elementary excitations are obtained from it through further spin reversals. Because, like vortex excitations in the triangular lattice Ising antiferromagnet, these elementary excitations are not produced singly by local spin flips, they are said to be fractionalised. Moreover, since one member of the pair is a source for the emergent gauge flux, and the other a sink, they form a monopole anti-monopole pair.

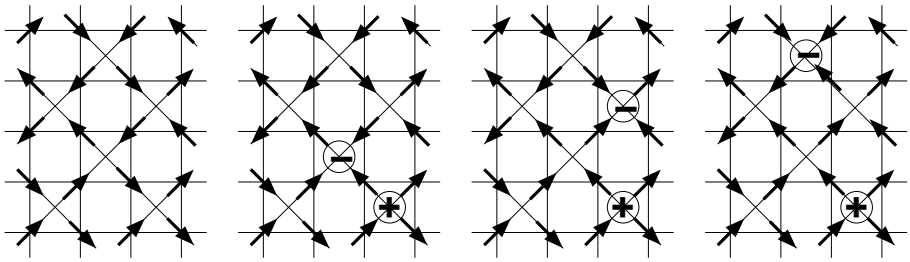

Figure 15: Generation of a monopole anti-monopole pair from ground state of two-dimensional spin ice, and their separation, by successive spin flips.

The energy of a monopole anti-monopole pair arising from exchange interactions is independent of their separation in a nearest neighbour model. There is, however, an entropic interaction between the pair, since the number of ground states available to the background spins depends on the separation r of the excitations. The entropic potential $V(r)$, as for monomers in the Coulomb phase of a three-dimensional dimer model on a bipartite lattice, is given by Eq. (30). Likewise, since the entropic cost of separating the pair to infinity is bounded, monopole excitations are deconfined.

4.4 Dipolar interactions

Our treatment of spin ice to this point has omitted the long-range part of dipolar interactions. Clearly, its inclusion will lift the high degeneracy of ground states of the nearest neighbour model, and one might expect that it would simply set an unwelcome limit on the physics we have discussed so far. Rather than being just a bug, however, dipolar interactions turn out to add a spectacular feature to spin-ice physics [38].

A very convenient framework for thinking about dipolar effects is provided by an approximation known as the dumbbell model. Here, in the first instance, magnetic dipoles μ of atomic size are replaced by 'dumbbells' of positive and negative magnetic charge $Q/2$ at a separation a equal to the distance between the centres of adjacent tetrahedra of the lattice. Setting the dipole moment of the dumbbell equal to the microscopic moment, the leading contribution to long-range interactions is captured exactly. The power of this description stems from the fact that, for all ground states of the nearest-neighbour model, the positive and negative magnetic charges at the centre of each tetrahedron cancel. In turn, this fact is a demonstration that the leading contribution to the energy from dipolar interactions is the same for all these states. Subleading terms follow from the multipole expansion and fall off with distance as r^{-5}. The estimated ordering temperature of spin-ice materials, $T_{\rm c} \lesssim 0.2\,\theta_{\rm CW}$, is rather low for that reason [39]. Such ordering is not observed under ordinary experimental conditions because spin dynamics is very slow at low temperature.

Turning to monopole excitations, the dumbbell model serves to expose a striking consequence of dipolar couplings, since dumbbell charges fail to cancel in tetrahedra that contain these quasiparticles. As a result, a well-separated monopole anti-monopole pair is subject to a Coulomb interaction

$$U(r) = -\frac{\mu_0 Q^2}{4\pi r} \tag{36}$$

of *magnetic* origin. The charge Q is related to the atomic dipole moment and the lattice spacing by $Q = 2\mu/a$, and the monopole chemical potential is fixed by the nearest-neighbour contributions to spin interactions. Note that while the entropic and dipolar contributions to monopole interactions (Eqns. 30 and 36) have the same dependence on separation, the entropic one makes a temperature-independent contribution to Boltzmann weights and so the dipolar one is dominant at low temperature. The magnetic Coulomb interaction between monopoles is a remarkable example of an emergent longer-range interaction $(1/r)$ arising from shorter-range $(1/r^3)$ microscopic interactions. It appears because of the interplay between these microscopic interactions and the correlations of the Coulomb

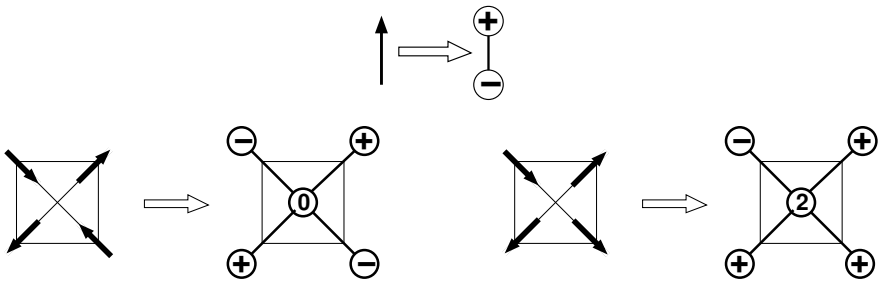

Figure 16: The dumbbell approximation. Dipoles are replaced with a dumbbell of opposite charges at finite separation, as shown at the top. If this separation is chosen to be the distance between tetrahedron centres, then two-in two-out tetrahedra are charge neutral (bottom left) but one-in three-out tetrahedra have net charge (bottom right).

phase, and it stands in contrast to the familiar situation (for example, in a plasma) in which correlations serve to screen long-range microscopic interactions, leaving only a short-range effective potential.

A second, and much more conventional, consequence of atomic dipole moments is that spins couple to an external magnetic field. To appreciate the form of this coupling, recall that moments are aligned along local crystal field axes, and that these are differently orientated on each of the four sublattices, as shown in Fig. 11. The Zeeman contribution to the Hamiltonian in the presence of a field $\vec{H}$ is therefore

$$\mathcal{H}_{\rm Z} = -\mu\mu_0 \sum_i [\vec{H} \cdot \hat{e}_i] S_i \,, \tag{37}$$

and so the strength of coupling to spins on different sublattices depends on the orientation of $\vec{H}$ relative to the crystal axes.

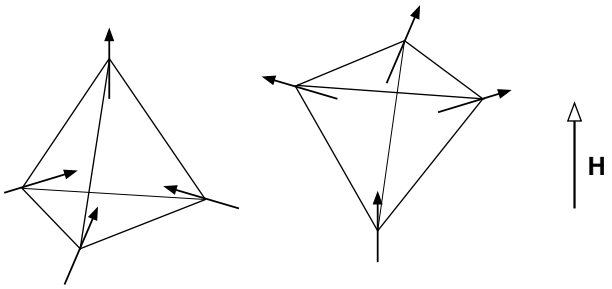

Figure 17: Spin configurations favoured by a $[111]$ field: magnetic charges $\pm Q$ are induced in tetrahedra on opposite sublattices.

This sublattice-dependent Zeeman coupling can be exploited to control monopole density in a way that provides rather direct evidence for magnetic Coulomb interactions. Specifically, a field directed along the $[111]$ axis acts as a staggered chemical potential for monopoles, favouring monopoles of charge Q in the tetrahedral on one sublattice of $\mathcal{B}$ and charge $-Q$ on the other sublattice, as indicated in Fig. 17. In this way, by varying field strength, one can drive a transition between low and high monopole density phases. Experimentally, this is observed to be first order. Theory for a charged system, and simulations including magnetic dipolar interactions reproduce this first-order transition, in contrast to theory and simulations for models with only nearest-neighbour interactions, where the transition is continuous [38].

5 Quantum spin liquids

We now turn to the quantum physics of frustrated magnets, where frustration is interesting particularly because it provides a mechanism that suppresses Néel order and promotes alternative, quantum-disordered phases.

5.1 Introduction

To understand that destruction of conventional order is likely in frustrated magnets, we can examine the reduction of ordered moments in the Néel state by zero-point fluctuations. Within the framework of harmonic spinwave theory, we start from a classical ground state for a spin model and choose axes at each site that have $\hat{z}$ oriented along the local ground-state spin direction. Using the Holstein-Primakoff transformation, spin operators are expressed in terms of bosonic ones via the relation $S^z_{\mathbf{r}} = S - a^\dagger_{\mathbf{r}} a_{\mathbf{r}}$. Fluctuations lower the ground-state moment $\langle S^z_{\mathbf{r}} \rangle = S - \Delta S$ by an amount $\Delta S \equiv \langle a^\dagger_{\mathbf{r}} a_{\mathbf{r}} \rangle$ that can be expressed as an average over contributions from each mode. The schematic form (details depend on the system) in terms of spinwave frequencies $\omega_{\mathbf{k}}$ and exchange interaction J is [40]

$$\Delta S \sim \frac{J}{\Omega} \int_{\mathrm{BZ}} \frac{\mathrm{d}^d \mathbf{k}}{\hbar \omega_{\mathbf{k}}}, \tag{38}$$

where Ω is the Brillouin zone (BZ) volume. As we have seen in Sec. 1.2, frustration promotes macroscopic classical ground-state degeneracy and branches of soft modes. Here we find that these modes make divergent contributions to ΔS, destabilising long range order.

Is the resulting state a quantum spin liquid? A necessary requirement is that (i) *the ground state leaves all symmetries of the Hamiltonian unbroken*, and the absence of Néel order is one aspect of this. To appreciate that we should demand more, consider as an example a bi-layer, square-lattice spin-half Heisenberg antiferromagnet, having nearest neighbour exchange J within layers and J' between layers. This model has two phases: the ground state is Néel ordered for $J' \ll J$, but consists of interlayer singlets for $J' \gg J$. Although the large J'/J state breaks no symmetries, it is 'ordinary' rather than 'exotic', in the sense that it is continuously connected to a band insulator. That is to say, there is a path in the space of Hamiltonians that connects this phase of the spin model to a tight-binding model without interactions, that has one filled band (symmetric under layer interchange) and one empty band (antisymmetric under interchange).

To exclude such ordinary possibilities, we make require in addition that a quantum spin liquid (ii) *has half odd-integer spin per unit cell*. The combination of (i) and (ii) together imply for a large class of models that a system with a gapped ground state has topological order, as we now discuss.

5.2 Lieb-Schultz-Mattis theorem

Some strong constraints on the nature of ground states and excitations in spin models that have half odd-integer spin per site and (at least) U(1) symmetry are revealed by the Lieb-Schultz-Mattis theorem [41]. It was originally proved for one-dimensional models, but has subsequently been applied to quasi-one dimensional and higher dimensional systems [42, 43]. The theorem shows for a chain of length L that the energy gap between the ground and first excited states vanishes as $L \to \infty$. We know of three distinct ways in which this can happen. Two of them are conventional. First, if the model spontaneously breaks a symmetry, the ground state belongs to a low-lying multiplet, and splittings within the multiplet vanish as L diverges. An example is a state in which the size of the unit cell is doubled spontaneously by spin dimerisation. Second, if the model has a branch of gapless excitations, the lowest excitation energy decreases as a power of system size. This is the case for spinon excitations in the spin-half Heisenberg chain. The third, unconventional possibility concerns systems that do not show symmetry breaking, and in which excitations that can be created by local operators are gapped. For these, the implication of the theorem is that the ground state belongs to a low-lying multiplet that does not originate from symmetry breaking. Instead, it has its origin in topological order.

We will sketch the proof as it applies to the spin-half XXZ chain, and then discuss more general implications. Consider the Hamiltonian

$$\mathcal{H} = J \sum_n \left\{ \frac{1}{2} [S^+_n S^-_{n+1} + S^-_n S^+_{n+1}] + \Delta S^z_n S^z_{n+1} \right\} \tag{39}$$

for a chain of L sites with periodic boundary conditions and L even. Suppose the ground state $|0\rangle$ is unique (if it is degenerate, there is nothing to prove, since the gap is zero) and denote its energy by E_0. We construct a second state $|\psi\rangle = U|0\rangle$ from it by acting with an operator

$$U = \exp\left(2\pi i \sum_{n=1}^{L} \frac{n}{L} S^z_n \right) \tag{40}$$

that generates a long-wavelength twist of spin configurations about the z-axis. We will show that $\langle \psi | 0 \rangle = 0$, and will use $\langle \psi | (\mathcal{H} - E_0) | \psi \rangle$ to obtain a variational bound on the separation in energy between the ground and first excited states of $\mathcal{H}$.

To show orthogonality of $|0\rangle$ and $|\psi\rangle$, consider the effect of translations on $|0\rangle$ and on $|\psi\rangle$. Let the operator T effect translation by one lattice spacing. We have $\mathrm{T}\,|0\rangle = |0\rangle$ since the ground state is unique. On the other hand

$$\mathrm{T}\,U\,\mathrm{T}^{-1} = U\,e^{-\frac{2\pi i}{L}\sum_n S^z_n}\,e^{2\pi i S^z_1}\,. \tag{41}$$

The factor $e^{-\frac{2\pi i}{L}\sum_n S^z_n} = +1$ if $\sum_n S^z_n = 0$ (and there is ground-state degeneracy if $\sum_n S^z_n \neq 0$), but for half-odd-integer spins the factor $e^{2\pi i S^z_1} = -1$. Hence $\mathrm{T}|\psi\rangle = -|\psi\rangle$, and therefore $\langle\psi|0\rangle = 0$.

In order to evaluate $\langle\psi|(\mathcal{H} - E_0)|\psi\rangle$, we first examine how U transforms a single spin operator. We have

$$e^{-i\theta S^z} S^+ e^{i\theta S^z} = e^{-i\theta} S^+ \quad \text{and so} \quad U^\dagger S^+_n S^-_{n+1} U = e^{2\pi i/L} S^+_n S^-_{n+1}\,. \tag{42}$$

From this we find

$$\langle\psi|(\mathcal{H} - E_0)|\psi\rangle = -\frac{J}{2}[1 - \cos(2\pi/L)] \sum_n \langle S^+_n S^-_{n+1} + S^-_n S^+_{n+1}\rangle\,. \tag{43}$$

Since the factor $[1 - \cos(2\pi/L)]$ decreases as $1/L^2$ while $\sum_n |\langle S^+_n S^-_{n+1} + S^-_n S^+_{n+1}\rangle| \leq 2L$, the energy gap separating E_0 from the next eigenstate vanishes at least as fast as $1/L$, which is the result we seek.

These ideas can most simply be extended to higher dimensions by considering a system on a strip, with the width M chosen to be an odd integer so that the spin per unit cell of the strip remains half odd-integer [42]. The bound on the energy gap implied by Eq. (43) is then $\mathcal{O}(M/L)$, which again vanishes provided we take the thermodynamic limit in an anisotropic fashion, a restriction not required in a more sophisticated approach [43].

The possibility of asymptotic degeneracy without symmetry breaking or gapless excitations is very striking. One route to understanding how it can arise is provided by quantum dimer models.

5.3 Quantum dimer models

5.3.1 RVB picture

In order to discuss spin liquid states we need a suitable language. It should provide an alternative to the picture we have of Néel order, which starts from a product wavefunction based on the classical ground state. Anderson's resonating valence bond (RVB) state [1, 44] offers this language: we describe the spin liquid wavefunction using a basis of short-range singlets. In one such basis state, each spin is paired with another nearby spin to form a singlet, with different basis states arising from different pairings. This idea is depicted in Fig. 18.

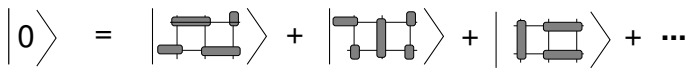

Figure 18: Schematic illustration of the RVB state as a superposition of short-range singlets.

Efforts to develop this picture directly face many difficult issues and questions [32]. Different basis states are not orthogonal, and it is not immediately apparent whether the basis is complete in the space of total singlets. Equally, one might ask what the prescription should be for choosing expansion coefficients, and how the Néel state can be written in this basis.

5.3.2 Quantum dimer models

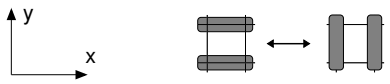

Figure 19: Resonance for quantum dimer model on square lattice.

Quantum dimer models [32] short-circuit many of these problems by defining a quantum-mechanical problem on a Hilbert space that has the correlations of a classical Coulomb phase built in from the start. The key idea is simply to define an orthonormal basis $\{|\mathcal{C}\rangle\}$ set to be the close-packed dimer coverings $\mathcal{C}$ of a given lattice, so that an arbitrary state in this space has the form $|\psi\rangle = \sum_{\mathcal{C}} A_{\mathcal{C}}|\mathcal{C}\rangle$. The other ingredient is a choice of Hamiltonian. In

general it will have 'potential' terms, which are diagonal in the dimer covering basis, and 'kinetic' terms, which are off-diagonal. The form proposed for the square lattice by Rokhsar and Kivelson [32] is

$$\mathcal{H} = \sum \{-t[\,|{=}\rangle\langle{\|}| + |{\|}\rangle\langle{=}|\,] + v[\,|{\|}\rangle\langle{\|}| + |{=}\rangle\langle{=}|\,]\}\ . \tag{44}$$

The notation used is intuitive although compact. Unpacking it: the sum runs over all elementary plaquettes of the lattice and the symbol $|{=}\rangle\langle{=}|$ denotes a projection operator onto states that have a horizontal pair of dimers in this plaquette. Similarly, the symbol $|{=}\rangle\langle{\|}|$ represents an operator that converts a horizontal pair of dimers in this plaquette to a vertical pair, and yields zero otherwise. It therefore produces the dimer resonances shown in Fig. 19.

Extensions to different lattices are straightforward. For example, on the triangular lattice one allows resonances of pairs of dimers on four-site plaquettes of three types, as shown in Fig. 20(a), while on the honeycomb lattice three-dimer resonances are required [Fig. 20(b)]. In general, one wants to include in the kinetic energy a set of resonances that is sufficient to connect all dimer configurations within a given U(1) or $\mathcal{Z}_2$ sector, but is otherwise as local as possible.

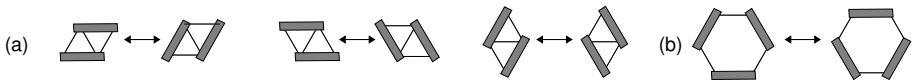

Figure 20: Resonances for quantum dimer models on (a) triangular and (b) honeycomb lattices.

The nature of the ground state of the quantum dimer model Hamiltonian (44) depends on the values of the parameters v and t. We will discuss only $t > 0$, so that the kinetic energy favours a nodeless wavefunction. A special role is played by the Rokhsar-Kivelson (RK) point in parameter space, $v = t$, because here the ground state wavefunction is given exactly by an equal-amplitude superposition $|\mathcal{G}\rangle$ of all dimer coverings within a given sector. To see this, note that the Hamiltonian at the RK point has a form

$$\mathcal{H}_{\rm RK} = t \sum \big(|{\|}\rangle - |{=}\rangle\big)\big(\langle{\|}| - \langle{=}|\big) \tag{45}$$

which is a sum of projectors with a positive coefficient. Its eigenvalues are therefore non-negative. Moreover $|\mathcal{G}\rangle$ is annihilated by the projection operators, and so is an eigenstate with energy zero. It is unique by the Perron-Frobenius theorem, provided the kinetic term is ergodic within the sector.

5.3.3 Correlations

Knowledge of the ground state wavefunction enables us to evaluate equal-time correlation functions. In particular, the ground state expectation value of an observable that is diagonal in the dimer basis is given by an average over dimer coverings. From this we can deduce at once that dimer correlations at the RK point of a quantum dimer model take the power-law form characteristic of a Coulomb phase [see Eqns. (26) and (29) for two and three dimensions, respectively] on bipartite lattices, and are exponentially decaying on non-bipartite lattices.

We can also consider the quantum dimer model in the presence of a pair of static monomers. At the RK point, equal amplitude superpositions of dimer coverings continue to define zero energy eigenfunctions, and so the ground state energy is independent of the separation between monomers. From this one concludes that monomers are deconfined in the ground state. Consider for comparison the behaviour at infinite temperature. In this limit (as discussed in Sec. 3) there is an entropic contribution to the monomer-monomer potential. It is weakly (logarithmically) divergent at large separations in two dimensions on bipartite lattices, giving confinement in this case. In other cases monomers are deconfined: the potential has the Coulomb form on three-dimensional bipartite lattices, and approaches its limiting value exponentially fast with separation on non-bipartite lattices in both two and three dimensions.

5.3.4 Phase diagram

Moving away from the solvable RK point, we would like to understand the ground-state phase diagrams of quantum dimer models on various lattices as a function of the dimensionless coupling v/t [32, 45, 46]. The behaviour in some regimes and limits is clear from simple arguments.

First, for $v > t$ we can write $\mathcal{H}$ in terms of the Hamiltonian $\mathcal{H}_{\rm RK}$ at the RK point and a non-negative remainder, as

$$\mathcal{H} = \mathcal{H}_{\rm RK} + (v - t) \sum \big\{|{\|}\rangle\langle{\|}| + |{=}\rangle\langle{=}|\big\}\,. \tag{46}$$

The so-called staggered state shown in Fig. 21(a) is annihilated by both terms in this Hamiltonian, and is hence the ground state for all $v > t$. In terms of the description of Coulomb phases on bipartite lattices, this is the state with maximal flux. It also has analogues on non-bipartite lattices: see Fig. 21(d).

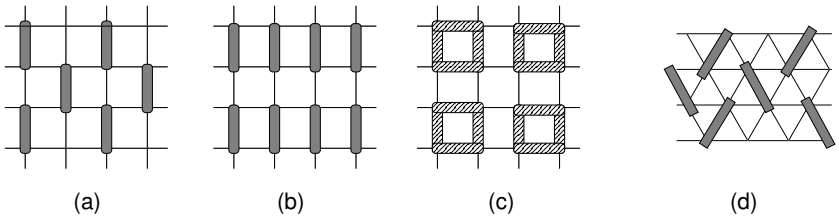

Figure 21: Some possible ordered phases for quantum dimer models: (a) staggered, (b) columnar and (c) plaquette states on the square lattice; (d) staggered state on the triangular lattice.

In the opposite limit, $v \to -\infty$, the ground state is a columnar state, maximising the number of flippable plaquettes, as illustrated in Fig. 21(b). Further possibilities at intermediate values of v/t include plaquette states, shown schematically for the square lattice in Fig. 21(c): in these states dimers resonate independently on different plaquettes between horizontal and vertical pairs.

Note that all of the states shown in Fig. 21 break spatial symmetries and are degenerate for that reason. By contrast, the ground state at the RK point leaves spatial symmetries intact; its degeneracy arises topologically, from the existence of different sectors, labelled by U(1) or $\mathbb{Z}_2$ quantum numbers according to the lattice type. The fact that they support a set of distinct ground states labelled by topological fluxes is a crucial feature of quantum dimer models, inherited from their classical counterparts. It illustrates how the degeneracy demanded by the Lieb-Schulz-Mattis theorem can arise without local symmetry breaking.

A full determination of the phase diagram requires Monte Carlo calculations. Here, quantum dimer models have a tremendous advantage over most spin Hamiltonians for frustrated systems, because they avoid the so-called sign problem and can be simulated efficiently using worm algorithms. The resulting phase diagrams are shown schematically in Fig. 22.

Some aspects of the phase diagram are generic, but others depend on spatial dimension and on whether or not the lattice is bipartite. Properties precisely at the RK point are known in all cases by reference to the corresponding classical dimer problem: dimers are disordered, with correlations that decay exponentially on non-bipartite lattices and as a power law on bipartite lattices. Moreover, the RK point lies at a phase boundary, since the staggered state is the ground state for all $v > t$. Crucial differences in behaviour appear on the other side of the RK point ($v < t$). A simple first step to rationalising these differences is to use classical, high-temperature properties as a basis for guessing the nature of the quantum ground state. Specifically, we know that the high-temperature, entropic interaction between monomers yields confinement on bipartite lattices in two dimensions, but not in three dimensions or on non-bipartite lattices. Correspondingly, the ground state of quantum dimer models is generically ordered on bipartite lattices in two dimensions. Deconfinement of monomers at the RK point on the square lattice must therefore be seen as a special feature of the transition between one ordered phase (the plaquette phase for $v < t$) and another (the staggered phase for $v > t$). In contrast, deconfinement of monomers at the RK point on the triangular or diamond lattices is a reflection of behaviour throughout a dimer liquid phase that extends from the RK point to smaller values of v/t. As we have seen in Sec. 3, topological order in this liquid phase is characterised respectively by $\mathbb{Z}_2$ and U(1) quantum numbers, which distinguish different sectors of the dimer configuration space, and therefore different quantum ground states.

A summary of the main features of the phase diagrams for quantum dimers models shown in Fig. 22 is that deconfined phases are found: (i) in both two and three spatial dimensions for $\mathbb{Z}_2$ models, which arise on non-bipartite lattices, and (ii) only in three spatial dimensions in U(1) models, which arise on bipartite lattices [45, 46]. These are general properties of lattice gauge theories: whereas $\mathbb{Z}_2$ theories support confined and deconfined phases in 2+1 and 3+1 dimensions, compact U(1) theories are known always to be confining in 2+1 dimensions, but to have both types of phase in 3+1 dimensions [47].

5.3.5 Excitations

Three types of excitation are important in quantum dimer models. Of these, monomers (mentioned already) involve a relaxation of the dimer covering constraint, while the others – visions and emergent photons – are excited states of complete dimer coverings, which are respectively point-like and wave-like.

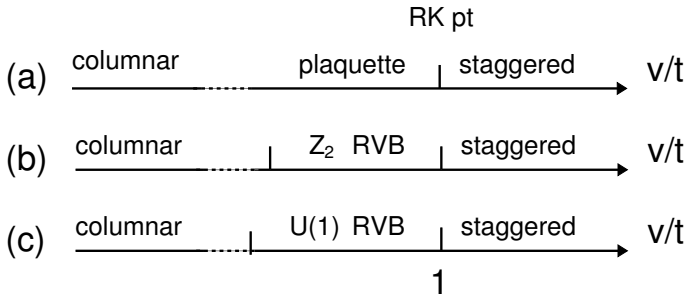

Figure 22: Schematic phase diagrams for the quantum dimer model on (a) square, (b) triangular and (c) diamond lattices.

The energy cost of introducing monomers is free parameter of the quantum dimer model, not fixed by the parameters v and t. It is natural, however, to regard them as gapped excitations, arising in pairs from breaking dimers. Viewing the dimer as a spin singlet, the monomer carries spin one-half and so is also referred to as a spinon. An isolated monomer in a dimer covering of a bipartite lattice is either a source or sink of U(1) flux, depending on which sublattice it occupies, and in that sense is a monopole. As we have discussed in Sec. 3.4, transitions between ground states in different topological sectors can be produced by generation of a pair of quasiparticles, followed by transport of one quasiparticle around the torus, and ending with recombination. The relevant quasiparticles here are monomer excitations.

Variational wavefunctions offer a language in which to discuss excitations of $\mathcal{H}_{\rm RK}$ within the space of close-packed dimer coverings. At the RK point we know that the ground state wavefunction has equal amplitude for all coverings within a given sector. An excited state wavefunction must have a phase that varies with dimer covering or it could not be orthogonal to this ground state.

The vison [48] is a vortex excitation of a two-dimensional system. It can be represented at the RK point by a variational wavefunction of the form

$$|\psi_{\rm vison}\rangle = \sum_{\mathcal{C}} (-1)^{n_{\mathcal{C}}} |\mathcal{C}\rangle \, . \tag{47}$$

Here $n_{\mathcal{C}}$ is the number of dimers in the configuration $\mathcal{C}$ that cross a line on the dual lattice which extends from the centre of the plaquette on which the excitation is based to the system boundary (or, for a system on a torus, to the centre of another vison), as illustrated in Fig. 23. In order for a wavefunction of this form to be reasonable, its physical properties should depend only on the line's endpoints, and not on the line's path: it is a simple exercise to check that this is true. To understand the significance of the form of this wavefunction, consider two configurations,

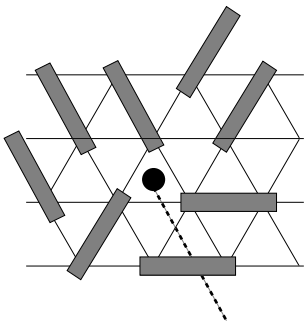

Figure 23: Vison excitation.

$\mathcal{C}$ and $\mathcal{C}'$, which are related by flipping dimers around a single loop. The dimer flip changes the sign of $(-1)^{n_{\mathcal{C}}}$ if the loop encloses the vison, but otherwise has no effect. This suggests several conclusions. First, far from the vison, the state $|\psi_{\rm vison}\rangle$ is very similar to $|\mathcal{G}\rangle$, since many different components of the wavefunction, related by dimer flips around loops that do not enclose the vison, contribute all with the same phase to $|\psi_{\rm vison}\rangle$, just as they do to $|\mathcal{G}\rangle$. Second, $|\psi_{\rm vison}\rangle$ and $|\mathcal{G}\rangle$ are orthogonal, since the average of $(-1)^{n_{\mathcal{C}}}$ over configurations is zero. Third, close to the vison, the states $|\psi_{\rm vison}\rangle$ and $|\mathcal{G}\rangle$ are quite different, and so we expect a finite energy gap for vison creation.

An emergent photon is an excitation involving density waves of the dimer orientations. It is a gapless excitation of a U(1) quantum dimer liquid, and so of interest at the RK point on bipartite lattices in 2+1 and 3+1 dimensions, and also away from the RK point in the U(1) phase in 3+1 dimensions. At the RK point itself, discussion of a trial wavefunction is again a very useful approach [32]. The excitation is characterised by a polarisation $\hat{\tau}$ and a wavevector $\mathbf{q}$. To specify the trial wavefunction we use the dimer number operator $\sigma_{\hat{\tau}}(\mathbf{r})$. Its Fourier transform is

$$\sigma_{\hat{\tau}}(\mathbf{q}) = \sum_{\mathbf{r}} e^{i\mathbf{q}\cdot\mathbf{r}} \sigma_{\hat{\tau}}(\mathbf{r}) \tag{48}$$

and the trial wavefunction we consider is

$$|\psi_{\text{photon}}\rangle = \sigma_{\hat{\tau}}(\mathbf{q})|\mathcal{G}\rangle\,. \tag{49}$$

Note that $\langle\mathcal{G}|\psi_{\text{photon}}\rangle = 0$ for $|\mathbf{q}| \neq 0$ since $|\mathcal{G}\rangle$ and $|\psi_{\text{photon}}\rangle = 0$ are both eigenstates of translation, but with different eigenvalues. In addition, for small $|\mathbf{q}|$ the state $|\psi_{\text{photon}}\rangle$ is locally similar to $|\mathcal{G}\rangle$, in the sense that dimer flips around short loops induce only small changes in the phases of its expansion coefficients $A_{\mathcal{C}}$.

Excitation energies $\mathcal{E}(\mathbf{q})$ in the quantum dimer model can be determined variationally using this trial wavefunction, taking inspiration from Feynman's treatment of phonon modes in Bose condensates [49]. We start from

$$\mathcal{E}(\mathbf{q}) \leq \frac{\langle\mathcal{G}|\sigma^\dagger_{\hat{\tau}}(\mathbf{q})\mathcal{H}_{\text{RK}}\sigma_{\hat{\tau}}(\mathbf{q})|\mathcal{G}\rangle}{\langle\mathcal{G}|\sigma^\dagger_{\hat{\tau}}(\mathbf{q})\sigma_{\hat{\tau}}(\mathbf{q})|\mathcal{G}\rangle} - \frac{\langle\mathcal{G}|\mathcal{H}_{\text{RK}}|\mathcal{G}\rangle}{\langle\mathcal{G}|\mathcal{G}\rangle} = \frac{f(\mathbf{q})}{2s(\mathbf{q})}\,, \tag{50}$$

where

$$f(\mathbf{q}) = \langle\mathcal{G}|[\sigma^\dagger_{\hat{\tau}}(\mathbf{q}),[\mathcal{H}_{\text{RK}},\sigma_{\hat{\tau}}(\mathbf{q})]]|\mathcal{G}\rangle \quad \text{and} \quad s(\mathbf{q}) = \langle\mathcal{G}|[\sigma^\dagger_{\hat{\tau}}(\mathbf{q})\sigma_{\hat{\tau}}(\mathbf{q})|\mathcal{G}\rangle\,.$$

From Eq. (50) we see that excitations are gapless if there are wavevectors $\mathbf{q}$ at which $f(\mathbf{q})$ vanishes and $s(\mathbf{q})$ remains finite or approaches zero more slowly. In turn, $f(\mathbf{q}) = 0$ if $[\mathcal{H}_{\text{RK}},\sigma_{\hat{\tau}}(\mathbf{q})] = 0$, and for the latter to hold we require both of the two dimer configurations shown in Fig. 19 to make the same contribution to $\sigma_{\hat{\tau}}(\mathbf{q})$. Setting $\hat{\tau} = \hat{x}$ for definiteness, this is the case in two dimensions if $q_y = \pi$, or in three dimensions if $q_y = q_z = \pi$. Writing $\mathbf{q} = (\pi,\pi) + \mathbf{k}$ or $\mathbf{q} = (\pi,\pi,\pi) + \mathbf{k}$, one finds $f(\mathbf{q}) \propto k_y^2$ or $f(\mathbf{q}) \propto k_y^2 + k_z^2$, respectively. It remains to compute $s(\mathbf{q})$, which is a correlator for classical dimer coverings and can be evaluated using the treatment of Coulomb phases established in Sec. 3. As dimer occupancy is represented by flux, we require the flux correlator; and because the mapping between dimers and fluxes uses an alternating orientation convention on links, long wavelength flux correlations reflect dimer correlations near the Brillouin zone corner. From the relation

$$\langle\mathcal{G}|[\sigma^\dagger_{\hat{x}}(\mathbf{q})\sigma_{\hat{x}}(\mathbf{q})|\mathcal{G}\rangle \propto \langle B^x(-\mathbf{k})B^x(\mathbf{k})\rangle \tag{51}$$

one finds $s(\mathbf{q}) \propto k_y^2/k^2$ in two dimensions, and $s(\mathbf{q}) \propto (k_y^2 + k_z^2)/k^2$ in three. This yields the important result

$$\mathcal{E}(\mathbf{q}) \leq ck^2\,, \tag{52}$$

with c a numerical constant, showing that the quantum dimer model has gapless excitations at the RK point.

We shall see that the quadratic dispersion shown in Eq. (52) reflects true behaviour, rather than simply providing an upper bound, but it is specific to the RK point and is replaced by a linear dispersion within the U(1) phase in 3+1 dimensions. To discuss the relevant physics, we consider how to extend the continuum description of Coulomb phases from classical systems in D space dimensions to quantum systems in $D+1$ space-time dimensions.

Taking $D = 2$, we require an imaginary time action for a height field $h(\mathbf{r},t)$ that is compatible with Eq. (52). The quadratic expression

$$S_{\text{RK}} = \frac{1}{2}\int \left\{[\partial_t h(\mathbf{r},t)]^2 + K^2\left[\nabla^2 h(\mathbf{r},t)\right]^2\right\} \mathrm{d}^2\mathbf{r}\,\mathrm{d}t \tag{53}$$

is implied. It yields for the Fourier transform of the height field the correlator

$$\langle|h(\mathbf{k},\omega)|^2\rangle = \frac{1}{(Kk^2)^2 + \omega^2} \tag{54}$$

and hence an equal-time correlator

$$\int \mathrm{d}\omega\,\langle|h(\mathbf{k},\omega)|^2\rangle \propto \frac{1}{Kk^2} \tag{55}$$

of the form required for the classical height model that describes dimer correlations in the ground state wavefunction at the RK point. This action is, however fine-tuned; adding further symmetry-allowed terms, we arrive at

$$S_{2+1} = \frac{1}{2}\int \left\{ [\partial_t h(\mathbf{r},t)]^2 + \rho_2 |\vec{\nabla} h(\mathbf{r},t)|^2 + K^2 \left[\nabla^2 h(\mathbf{r},t)\right]^2 - g\cos 2\pi h(\mathbf{r},t) \right\} \mathrm{d}^2\mathbf{r}\,\mathrm{d}t\,.$$

We can identify the stiffness ρ_2 with the parameter combination $1 - v/t$ in the quantum dimer model. At the RK point the stiffness vanishes, g is irrelevant under renormalisation, and we return to Eq. (53). On one side of the RK point, $v > t$, ρ_2 is negative, promoting a state with a large gradient $|\vec{\nabla} h(\mathbf{r},t)|$ in the height field: the staggered phase. On the other side, $v < t$, positive ρ_2 suppresses fluctuations of $h(\mathbf{r},t)$ and $g\cos 2\pi h(\mathbf{r},t)$ is relevant, producing a pinned phase. In this way we see that the RK point for a bipartite lattice in 2+1 dimensions is an isolated critical point between two conventional ordered phases.

Contrastingly, quantum dimer models on bipartite lattices in 3+1 dimensions generically support a dimer liquid phase. Again we require an imaginary time action compatible with Eq. (52), now expressed in terms of the vector potential $\vec{A}(\mathbf{r},t)$. Picking the Coulomb gauge $\vec{\nabla}\cdot\vec{A}(\mathbf{r},t) = 0$, an expansion in space and time derivatives gives

$$S_{3+1} = \frac{1}{2}\int \left\{ |\partial_t \vec{A}(\mathbf{r},t)|^2 + \rho_2 |\vec{\nabla}\times\vec{A}(\mathbf{r},t)|^2 + K^2 |\vec{\nabla}\times[\vec{\nabla}\times\vec{A}(\mathbf{r},t)]|^2 \right\} \mathrm{d}^3\mathbf{r}\mathrm{d}t\,. \tag{56}$$

Again we expect $\rho_2 \propto 1 - v/t$. At the RK point, with $\rho_2 = 0$, we recover a quadratic dispersion relation for excitations, and equal-time correlations of the classical Coulomb phase. On one side of the RK point, with $v > t$, negative ρ_2 drives the system into a staggered phase, as in 2+1 dimensions. On the other side, however, with $v < t$, by introducing a scalar potential $\Phi(\mathbf{r},t)$ and writing $\vec{E}(\mathbf{r},t) = \partial\vec{A}(\mathbf{r},t) - \vec{\nabla}\Phi(\mathbf{r},t)$, the action can be expressed in the form [50, 51]

$$S_{3+1} = \frac{1}{2}\int \left\{ |\vec{E}(\mathbf{r},t)|^2 + \rho_2 |\vec{B}(\mathbf{r},t)|^2 + K^2 |\vec{\nabla}\times\vec{B}(\mathbf{r},t)|^2 \right\} \mathrm{d}^3\mathbf{r}\mathrm{d}t\,, \tag{57}$$

familiar from quantum electrodynamics. Weak perturbations to this action allowed by symmetry are irrelevant in the renormalisation-group sense. It describes a liquid phase of the quantum dimer model and has linearly dispersing emergent photon excitations. Monomers introduced into the dimer covering are monopole sources for the $\vec{B}$ field, and the three-dimensional analogue of visons are sources for the $\vec{E}$ field.

6 Concluding remarks

The presentation has necessarily been a very selective one, chosen particularly to bring out common strands in the treatment of frustration in classical models and in quantum systems. It is reassuring to find that the main ideas also emerge from quite different treatments.

6.0.6 Slave particles

A large and important class of theories follows from representing spins in terms of particles subject to a local constraint. The constraint can be imposed using a gauge field, which takes the same place in a description of a spin liquid as the gauge fields that appear in dimer models. One starting point is Schwinger's representation of spin-S operators using two species of bosons, as [40]

$$S^z = \frac{1}{2}(b_1^\dagger b_1 - b_2^\dagger b_2), \quad S^+ = b_1^\dagger b_2 \quad \text{and} \quad S^- = b_2^\dagger b_1\,, \tag{58}$$

with $[b_i b_j^\dagger] = \delta_{ij}$ and the constraint $b_1^\dagger b_1 + b_2^\dagger b_2 = 2S$. Fluctuations can be controlled by generalising from SU(2) to SU(N) [52], or on non-bipartite lattices to Sp(N) [53], and from two to N species of boson.

Alternatively, we can recall the origin of local moments in itinerant fermions [54], writing

$$\vec{S}_i = f_{i\alpha}^\dagger \vec{\sigma}_{\alpha\beta} f_{i\beta} \quad \text{with} \quad f_{i\uparrow}^\dagger f_{i\uparrow} + f_{i\downarrow}^\dagger f_{i\downarrow} = 1\,, \tag{59}$$

where $\{f_{i\alpha}^\dagger, f_{j\beta}\} = \delta_{ij}\delta_{\alpha\beta}$. The Heisenberg exchange term $\vec{S}_i \cdot \vec{S}_i$ then corresponds to a four-fermion interaction, and a mean-field decoupling leads to a quadratic fermion Hamiltonian of the form

$$\mathcal{H}_{\mathrm{MF}} = \sum_{ij,\sigma} \left\{ t_{ij} f_{i\sigma}^\dagger f_{j\sigma} + \left(\Delta_{ij} f_{i\uparrow}^\dagger, f_{j\downarrow}^\dagger + \text{h.c.} \right) \right\}\,, \tag{60}$$

where the hopping coefficients t_{ij} and pairing amplitudes Δ_{ij} serve as variational coefficients. Denoting the ground state of $\mathcal{H}_{\rm MF}$ by $|\text{Slater}\rangle$, components with double site occupancy can be removed by Gutzwiller projection to yield a spin liquid wavefunction

$$|\mathcal{G}\rangle = \prod_i (1 - n_{i\uparrow} n_{i\downarrow}) \, |\text{Slater}\rangle \, . \tag{61}$$

Within this approach, depending on the phases of the hopping amplitudes, the fermions move in a $\mathbb{Z}_2$, U(1) or SU(2) gauge field, and have a gapped, Dirac or metallic spectrum – in decreasing order of stability. Spinons are represented by Bogoliubov quasiparticles, and visions by flux excitations encoded in the phases of the hopping amplitudes [55].

6.0.7 Numerics

Unbiased numerical methods play a key role in this research field, and often represent the only way to find out what phases are supported by a particular physical model; Refs. [56] and [57] provide recent reviews. In general, while exact diagonalisation of the many-body Hamiltonian has the advantages of flexibility (for example, providing an early identification of a gapped spin liquid [58]), alternative techniques are important to avoid the difficulties stemming from the exponential growth with system size of the Hilbert space dimension. These include the design of Hamiltonians that avoid Monte Carlo sign problems [57], and the use of the density matrix renormalisation group and related methods to study quasi-one dimensional samples (see, for example [60]). At the same time, new approaches to identifying exotic states are increasingly important, such as the evaluation of entanglement entropy to probe topological order [59].

6.1 Summary

Some common strands run through much of the physics that has been presented. Frustration gives rise to classical degeneracy, and the correlations that are built onto these classical degenerate states lead to the ideas of topological sectors and deconfined, fractionalised excitations. By adding quantum dynamics to dimer models, two important types of stable quantum liquid phase can be realised. One is a gapped $\mathbb{Z}_2$ phase, stable in both two and three spatial dimensions, which has point-like excitations of two types: spinons and visons. The other is the U(1) liquid, stable only in three spatial dimensions, and having gapped electric and magnetic monopole excitations as well as gapless emergent photon modes. Models realising $\mathbb{Z}_2$ phases include, in two dimensions, the triangular lattice quantum dimer model [45], the toric code [61], and the spin-half kagome lattice Heisenberg antiferromagnet [62]. Examples of U(1) liquids are provided by the diamond lattice quantum dimer model [63] and by hard-core bosons on the pyrochlore lattice [64].

Acknowledgements

I am very grateful to all my collaborators in this field, and especially to Eugene Shender, Peter Holdsworth and Roderich Moessner. I acknowledge financial support from EPSRC.

References

[1] P. W. Anderson, Mat. Res. Bull. **8**, 153 (1973).

[2] A. P. Ramirez, Ann. Rev. Mater. Sci. **24**, 453 (1994).

[3] P. A. Lee, Science **321**, 1306 (2008).

[4] L. Balents, Nature **464**, 199 (2010).

[5] C. Lacriox, P. Mendels, and F. Mila (Eds.) *Introduction to Frustrated Magnetism*, Springer (2011).

[6] J. Villain, Z. Phys. B **33**, 31 (1979).

[7] B. Martinez, F. Sandiumenge, A. Rouco, A. Labarta, J. Rodriguezcarvajal, M. Tova, M. T. Causa, S. Gali and X. Obradors, Phys. Rev. B **46**, 10786 (1992).

[8] S.-H. Lee, C. Broholm, G. Aeppli, A. P. Ramirez, T. G. Perring, C. J. Carlile, M. Adams, T. J. L. Jones and B. Hessen, Europhys. Lett. **35**, 127 (1996).

[9] T. Fennell, P. P. Deen, A. R. Wildes, K. Schmalzl, D. Prabhakaran, A. T. Boothroyd, R. J. Aldus, D. F. McMorrow, and S. T. Bramwell, Science **326**, 415 (2009).

[10] T.-H. Han, J. S. Helton, S. Chu, D. G. Nocera, J. A. Rodriguez-Rivera, C. Broholm, and Y. S. Lee, Nature **492**, 406 (2012).

[11] S. Yamashita , Y. Nakazawa, M Oguni, Y. Oshimi, H. Nojiri, Y. Shimizu, K. Miyagawa, and K. Kanoda, Nat. Phys. **4**, 459 (2008).

[12] L. Pauling, *The Nature of the Chemical Bond* (Cornell Univ. Press, Ithaca, New York, 1945).

[13] A. P. Ramirez, A. Hayashi, R. J. Cava, R. Siddharthan, and B. S. Shastry, Nature **399**, 333 (1999).

[14] J. C. Maxwell, Philos. Mag. **27**, 294 (1864).

[15] J. N. Reimers, A. J. Berlinsky, and A.-C. Shi, Phys. Rev. B **43**, 865 (1991).

[16] R. Moessner and J. T. Chalker, Phys. Rev. Lett. **80**, 2929 (1998); Phys. Rev. B **58**, 12049 (1998).

[17] J. Villain, R. Bidaux, J. P. Carton, and R. J. Conte, J. Phys. Paris **41**, 1263 (1980).

[18] E. F. Shender, Sov. Phys. JETP **56**, 178 (1982).

[19] J. T. Chalker, P. C. W. Holdsworth, and E. F. Shender, Phys. Rev. Lett. **68**, 855 (1992).

[20] A. G. Gukasov, T. Brückel, B. Dorner, V. P. Plakhty, W. Prandtl, E. F. Shender, and O. P. Smirnov, Europhys. Lett. **7**, 83 (1988).

[21] T. Brückel, B. Dorner, A. G. Gukasov, V. P. Plakhty, Phys. Lett. A **162**, 357 (1992).

[22] M. E. Zhitomirsky, M. V. Gvozdikova, P. C. W. Holdsworth, and R. Moessner, Phys. Rev. Lett. **109**, 077204 (2012); L. Savary, K. A. Ross, B. D. Gaulin, J. P. C. Ruff, and L. Balents, Phys. Rev. Lett. **109**, 167201 (2012).

[23] D. A. Garanin and B. Canals, Phys. Rev. B **59**, 443 (1999); B. Canals and D.A. Garanin, Can. J. Phys. **79**, 1323 (2001).

[24] S. V. Isakov, K. Gregor, R. Moessner, and S. L. Sondhi, Phys. Rev. Lett. **93**, 167204 (2004).

[25] G. Wannier, Phys. Rev. **79**, 357 (1950); R. M. F. Houtappel, Physica **16** 425 (1950).

[26] H. W. J. Blöte and H. J. Hilhorst, J. Phys. A **15**, L631 (1982); B. Nienhuis, H. J. Hilhorst, and H. W. Blöte, *ibid.* **17**, 3559 (1984); B. Nienhuis, Phys. Rev. Lett. **49**, 1062 (1982).

[27] C. Zeng and C. L. Henley, Phys. Rev. B **55**, 14 953 (1997).

[28] M. E. Fisher, Phys. Rev. **124**, 1664 (1961); P. W. Kastelyn, Physica **27**, 1209 (1961).

[29] R. Kenyon, *An introduction to the dimer model*, Lecture Notes, arXiv:math/0310326.

[30] C. L. Henley, J. Stat. Phys. **89**, 483 (1997).

[31] D. A. Huse, W. Krauth, R. Moessner, and S. L. Sondhi, Phys. Rev. Lett. **91**, 167004 (2003).

[32] D. S. Rokhsar and S. A. Kivelson, Phys. Rev. Lett. **61**, 2376 (1998).

[33] P. Fendley, R. Moessner, and S.L. Sondhi, Phys. Rev. B 66, 214513 (2002).

[34] S. T. Bramwell and M. J. P. Gingras, Science **294**, 1495 (2001).

[35] M. J. Harris, S. T. Bramwell, D. F. McMorrow, T. Zeiske and K. W. Godfrey, Phys. Rev. Lett. **79**, 2554 (1997).

[36] C. L. Henley, Ann. Rev. Condens. Matter Phys., **1**, 179 (2010).

[37] P. H. Conlon and J. T. Chalker, Phys. Rev. B **81**, 224413 (2010).

[38] C. Castelnovo, R. Moessner, and S. L. Sondhi, Nature **451**, 42-45 (2008).

[39] R. G. Melko and M. J. P. Gingras, J. Phys.: Condens. Matter **16**, R1277 (2004).

[40] A. Auerbach, *Interacting electrons and quantum magnetism*, Springer (1998).

[41] E. H. Lieb, T. D. Schultz, and D. C. Mattis, Ann. Phys. **16**, 407 (1961).

[42] I. Affleck, Phys. Rev. B **37**, 5186 (1988).

[43] M. B. Hastings, Phys. Rev. **69**, 104431 (2004).

[44] P. W. Anderson, Science **235**, 1196 (1987).

[45] R. Moessner and S. L. Sondhi, Phys. Rev. Lett. **86**, 1881 (2001).

[46] R. Moessner and K. Raman, *in* Ref. [5].

[47] J. B. Kogut, Rev. Mod. Phys. **51**, 659 (1979).

[48] T. Senthil and M. P. A. Fisher, Phys. Rev. B **62**, 7850 (2000).

[49] R. P. Feynman, Phys. Rev. **94**, 262 (1954).

[50] R. Moessner and S. L. Sondhi, Phys. Rev. B **68**, 184512 (2003).

[51] M. Hermele, M. P. A. Fisher and L. Balents, Phys. Rev. B **69**, 064404 (2004).

[52] N. Read and S. Sachdev, Phys. Rev. Lett. **62**, 1694 (1989).

[53] N. Read and S. Sachdev, Phys. Rev. Lett. **66**, 1773 (1991).

[54] J. B. Marston and I. Affleck, Phys. Rev. B **39**, 11539 (1989).

[55] X. G. Wen, Phys. Rev. Phys. B **65**, 165113 (2002); P. Lee, N. Nagaosa, and X.-G. Wen, Rev. Mod. Phys. **78**, 17 (2006).

[56] A. M. Läuchli, *in* Ref. [5].

[57] A. W. Sandvik, AIP Conf. Proc. **1297**,135 (2010).

[58] G. Misguich, C. Lhuillier, B. Bernu, and C. Waldtmann, Phys. Rev. B **60**, 1064 (1999).

[59] S. V. Isakov, R. G. Melko, and M. B. Hastings, Science **335**, 193 (2012).

[60] M. S. Block, R. V. Mishmash, R. K. Kaul, D. N. Sheng, O. I. Motrunich, and M. P. A. Fisher, Phys. Rev. Lett. **106**, 046402 (2011).

[61] A. Yu. Kitaev, Ann. Phys. **303**, 2 (2003).

[62] S. Yan, D. A. Huse, and S. R. White, Science **332**, 1173 (2011); S. Depenbrock, I. P. McCulloch, and U. Schollwoeck, Phys. Rev. Lett. **109**, 067201 (2012); H.C. Jiang, Z. Wang, and L. Balents, Nature Physics **8**, 902 (2012).

[63] O. Sikora, F. Pollmann, N. Shannon, K. Penc, and P. Fulde, Phys. Rev. Lett. **103**, 247001 (2009).

[64] A. Banerjee, S. V. Isakov, K. Damle, Y. B. Kim, Phys. Rev. Lett. **100**, 047208 (2008).